Aus der Kinderchirurgischen Klinik und Poliklinik
im Dr. von Haunerschen Kinderspital
Klinik der Universität München
Direktor: Professor Dr. med. Oliver Muensterer

In silico drug repurposing identifies mebendazole as a treatment option for chemoresistant hepatoblastoma

Dissertation
zum Erwerb des Doktorgrades der Medizin
an der Medizinischen Fakultät der
Ludwig-Maximilians-Universität zu München

vorgelegt von
Qian Li
aus
Zhengzhou, China

Jahr
2023

Mit Genehmigung der Medizinischen Fakultät
der Universität München

Berichterstatter:	Prof. Dr. Roland Kappler
Mitberichterstatter:	PD Dr. Simon Hohenester PD Dr. Sebastian Pratschke PD Dr. Eberhard Lurz
Mitbetreuung durch den promovierten Mitarbeiter:	Dr. Salih Demir
Dekan:	Prof. Dr. med. Thomas Gudermann
Tag der mündlichen Prüfung:	26.10.2023

Contents

Introduction 4

1. Hepatoblastoma 4
1.1 Epidemiology 4
1.2 Clinical presentation 4
1.3 Diagnosis 4
1.4 Disease stage 5
1.5 Chemotherapy treatment for HB 5
2. Genetics and transcriptomics 6
3. Connectivity map 6
4. Aim of the study 6

Materials 8

1. Cell lines 8
2. Cell culture materials 8
3. Antibodies 9
4. Kits 9
5. Buffers and solutions 9
6. Chemicals reagents 11
7. Equipment 11
8. Software 12

Methods 13

1. Cell culture 13
2. MTT assay 13
3. Wound healing assay 13
4. Proliferation assay 13
5. Colony formation assay 14
6. Spheroid formation assay 14
7. Cell cycle analysis 14
8. Immunofluorescence 14
9. Apoptosis assay 14
10. RNA sequencing 15
11. Western blot 15
12. Synergy assay 15
13. Animal studies 15
14. Statistical analysis 16

Results **17**
1. The identification of MBZ as a candidate drug for HB 17
2. MBZ inhibits pediatric liver cancer cells viability 17
3. MBZ decreases migration of HB cells 18
4. MBZ inhibits HB cell short-term proliferation 19
5. MBZ inhibits HB cell long-term proliferation 20
6. MBZ reduces the growth of spheroid 22
7. MBZ disrupts spindle formation 22
8. MBZ induces G2/M arrest in the cell cycle 23
9. MBZ induces HB cell apoptosis 24
10. MBZ is involved in dysregulation of gene expression associated with cell growth and cell cycle regulation 24
11. MBZ combined with cisplatin exhibited synergistic activity in HB cells 26
12. MBZ inhibits tumour growth of HB cells in a mouse model 27

Discussion **29**

Summary **32**

ZUSAMMENFASSUNG **32**

Acknowledgment **32**

References **36**

Lebenslauf **43**

Table of Figures

Figure 1. Drug identification. 17
Figure 2. Cell viability after MBZ treatment at various concentrations. 18
Figure 3. MBZ inhibited invasion. 19
Figure 4. MBZ significantly inhibited proliferation. 20
Figure 5. MBZ inhibits long-term cell proliferation. 21
Figure 6. MBZ reduces the growth of spheroid. 22
Figure 7. MBZ induces disarrayed microtubules and abnormal spindles. 23
Figure 8. MBZ induces G2/M arrest in the cell cycle. 23
Figure 9. MBZ induces HB cell apoptosis. 24
Figure 10. MBZ is involved in dysregulation of gene expression associated with cell growth and cell cycle regulation. 25
Figure 11. MBZ in combination with the standard of care treatment. 27
Figure 12. MBZ inhibits tumour growth *in vivo*. 27

Table of Supplements

Supplementary Table S1. Top 50 up and down regulated genes according to the log2fold change. 34

Introduction

1. Hepatoblastoma

1.1 Epidemiology

After neuroblastoma and Wilms' tumour, hepatoblastoma (HB) is the most common type of malignant tumour in children, accounting for about 0.8-2.0% of malignant solid tumours [1]. It develops in children less than the age of 5 years old [2], most primarily 2 years old [3]. The ratio of males to females is 1.5:1 [2][4]. Most HBs are usually solitary. As with most tumours, the etiology of HB is still unclear. The occurrence and progression of HB are affected by environmental factors, especially some pathological factors during pregnancy, such as obesity, preeclampsia, gestational hypertension, polyhydramnios, and also some other reasons, like gonadotropin application, maternal oral contraceptives, heavy drinking and smoking [5]. Babies born with a low birth weight and premature babies have a higher risk of developing into HB [6][7]. Children who had certain genetic conditions, like hemihypertrophy, Beckwith Wiedemann syndrome, trisomy 18 [8], and familial adenomatous polyposis, are also more susceptible to HB [9].

1.2 Clinical presentation

HB symptoms can vary according to the tumour's size and whether it has spread or not. Some may have mild anemia, but usually have no other symptoms. Others have additionally clinical symptoms such as abdominal pain, nausea, vomiting, loss of appetite, and disorientation. Venous distention in the abdominal wall, jaundice, ascites, fever, anemia, and a rise in body weight are all possible signs in the later stages of HB [2][10]. In a minority of patients, precocious puberty may occur due to human chorionic gonadotropin secretion [10][11]. If the tumour presses on the nerve, this situation may result in back pain. In the late stages, if the abdominal tumour is large, it may cause difficulty in breathing.

1.3 Diagnosis

Ultrasound examination is the most convenient and first tool to diagnose HB [10]. Tumours often present as a single mass with clear edges, but sometimes also as multiple lesions in the liver.

The biomarker alpha-fetoprotein (AFP) is usually utilized to prove the existence of liver cancer. According to reports, the typical level of AFP in children is less than 50 nanograms per milliliter (ng/ml), while in adults, it is 10 ng/ml. HB is significantly indicated by an AFP level greater than 500 ng/ml [11][12]. Infants' AFP levels are relatively high at birth, but by the second year of life, they decrease to normal adult levels. AFP levels may be physiologically raised, and will not adequately reflect the diagnosis and burden of the disease, making the identification of a liver mass that manifests in the first few months of life a little bit more difficult. Thus, the final diagnosis requires obtaining tissue for pathological examination. The current method is

mainly needle biopsy, and even surgical tissue removal is required. Therefore, the comprehensive diagnosis of HB usually relies on imaging examinations, laboratory examinations, and pathological examinations.

1.4 Disease stage

The staging system of HB is based on the achievements of four trial groups: The International Childhood Tumor Strategy Group (SIOPEL), the Children Oncology Group (COG), the German Society for Pediatric Oncology and Haematology (GPOH), and the Japanese Study Group for Pediatric Liver Tumors (JPLT). The four organizations defined the criteria for risk classification and the approach for treating HB patients [13]. It is mainly based on the radiological assessment of the so-called pre-treatment extent of disease staging system (PRETEXT), that mainly takes the size and location of the tumour in the liver into account. Moreover, it assesses risk factors, such as patients' age, the alpha-fetoprotein levels in their serum, presence of metastases, vascular invasion, contiguous extrahepatic extension, multifocality and tumour rupture at diagnosis [14] [15].

According to these parameters above, it divides HB patients into four risk groups [13][15]，including very low, low, medium, and high risk. Patients at preoperative PRETEXT stage I, II, III with age ≥ 8 or with metastatic disease, and at preoperative PRETEXT stage IV with age ≥ 3 are usually defined as high risk. At present, alpha-fetoprotein lower than 100ug/L is also defined as a relatively poor prognostic factor.

1.5 Chemotherapy treatment for HB

Although surgery is still the main treatment for HB, the advent of chemotherapy has undoubtedly increased the resectable rate of HB and reduced the surgical rate. Chemotherapy for HB originated in the 1970s. The chemotherapy regimen for HB in the early period was not satisfactory. Over the past 30 years, some breakthroughs in treatment, in particular in the fields of chemotherapy, surgery and the development of orthotopic liver transplantation for locally inoperable disease [16], have significantly boosted the survival rate for HB in children. Recent studies have shown that children receiving chemotherapy and surgery had a five-year event-free survival rate of between 75 and 90 percent [17][18]. However, chemoresistant tumours are often associated with incomplete surgical resection and therefore poor outcome [19].

The introduction of cisplatin and doxorubicin has led to significant improvements in the outcomes of these children and was clearly advantageous over prior chemotherapy regimens which largely consisted of cyclophosphamide, vincristine, and fluorouracil (FU). Other chemotherapeutic agents (vincristine, FU, carboplatin, etoposide, ifosfamide, and irinotecan) have been used to treat newly diagnosed HB in the pediatric population [20][21][22]. But these therapeutic regimens are still being confronted with many challenges, especially in the aspect of minimizing long-term treatment-related toxicities such as cardiotoxicity, nephrotoxicity, and ototoxicity [23]. Thus, in view of the poor survival rates and significant toxicities that patients experience with conventional chemotherapy, novel compounds and therapeutic options are urgently needed.

2. Genetics and transcriptomics

Cytogenetic changes occur very frequently in HB and most cases affect chromosomes 2, 8, and 20 by gain and chromosomes 4 and 18 by loss [24]. The most commonly affected gene is CTNNB1, which is mutated in up to 90% of HB cases [25]. CTNNB1 encodes the protein β-catenin, which, in addition to helping cells adhere and communicate with each other, is mainly involved in Wnt signaling pathway [26]. Among other things, in embryonic development, cell proliferation and differentiation, Wnt signaling pathway plays a major role [27]. Mutations in CTNNB1 lead to accumulation of β-catenin and induction of target gene expression in the nucleus, resulting in uncontrolled activity of Wnt signaling pathway [28]. In addition to CTNNB1, other gene mutations of Wnt signaling pathway in HB have also been reported, which control the degradation of β-catenin and thus lead to a similar activation of the signaling pathway. Among them were APC mutations, which occur either as a germline mutation associated with familial adenomatous polyposis or as a somatic mutation [29]. However, cases with AXIN1 and AXIN2 mutations have also been detected in some HB patients [30].

More important is that 16-gene signature was identified to assist patient's stratification at diagnosis [15]. The 16-gene classification system divides cancers into two subgroups: well-differentiated cancers (C1), which have a good prognostic value, and poorly differentiated cancers (C2), which have a poor prognostic value [15][31]. Using this genetic profile and detailed clinical trials, molecular classification of HB may become a biomarker in the future.

3. Connectivity map

Genomic data have been used to repurpose new antitumour drugs. It is economical and efficient to use comparison of gene differential expression to repurpose drugs [32]. On the basis of intervening gene expression, the Broad Institute created the Connectivity Map, a database for gene expression profiling, which is utilized to identify functional connections between genes, disease states, and small molecule drugs [33]. It includes the gene expression patterns of MCF7, PC3, SKMEL5, and HL60 cell lines. 1,309 compounds were applied to treat these four cell lines at various concentrations at different times, which resulted in 6,100 instances [34][35]. Each instance was assigned, and perturbations are ranked by connectivity scores ranging from -1 to 1. The positive connectivity values at the top are the ones that correlate most strongly with the query signature, indicating that the drugs are capable of inducing the input signature. On the contrary, the strongest anticorrelations are found in the negative connectivity scores at the bottom, indicating that drugs have a greater similarity to the perturbagen than the current query signature [36]. Thus, CMap is a useful tool to predict new therapeutic options.

4. Aim of the study

In patients with hepatoblastoma, incomplete surgical resection and poor outcomes are common if the tumour does not respond to preoperative chemotherapy. The goal of this study is to explore new drug candidates for chemoresistant hepatoblastoma by integrating the Connectivity Map drug prediction tool with

patient transcriptomic and treatment response data. The most promising candidate drug should be tested on an *in vitro* testing platform of hepatoblastoma models for its efficacy and the tumour biological consequences on viability, cell cycle, apoptosis, sphere formation, and migration monitored in appropriate assays. Consequently, the experimentally validated drug should be tested *in vivo* using a mouse model of patient-derived xenografts.

Materials

1. Cell lines

HepT1, Homosapiens, HB	Pietsch et al. [37]
HUH6, Homosapiens, HB	JCRB,Osaka, Japan
Hep3B, Homosapiens, HB	Manassas, USA
HUH7, Homosapiens, HCC	JCRB,Osaka, Japan
HepG2, Homosapiens, HCCATCC	Manassas, USA
XenTech, Evry, France	
PDX cell line 282	
PDX cell line303	
PDX cell line284	
PDX cell line243	
PDX cell line279	
PDX cell line295	

2. Cell culture materials

Mebendazole	Selleckchem, Chesterbrook, PA, USA
Ultra-low attachment round bottom 96-well plate	Corning, Corning, NY, USA
Cell scraper	Sarstedt AG & Co., Nümbrecht, Germany
µ-slide 8-well chambered coverslips	Ibidi, Gräfelfing, Germany
DMEM/F12	Life Technologies, Carlsbad, CA, USA
L-glutamine	Thermo Fisher, Waltham, MA, USA
Corning GmbH, Wiesbaden, Germany	
Costar Stripette Serologic Pipettes 5ml	
Costar Stripette Serologic Pipettes 10ml	
Costar Stripette Serologic Pipettes 25ml	
Invitrogen, Karlsruhe, Germany	
RPMI	
Penicillin-Streptomycin (PS)	
DPBS	
Fetal bovine serum (FCS)	
Trypsin-EDTA 0.05%	
Sarstedt AG & Co., Nümbrecht, Germany	

Biosphere Filtertips 1-10 µl
Biosphere Filtertips 10-100 µl
Biosphere Filtertips 100-1000 µl
NUNC, Langenselbold, Germany
Cell culture T-Flasks 25cm^2
Cell culture T-Flasks 75cm^2
Petri dishes 100mm
6-well Plates, non-pyrogenic
12-well Plates, non-pyrogenic
24-well Plates, non-pyrogenic
96-well Plates, non-pyrogenic

3. Antibodies

Anti-α-tubulin, mouse	Sigma-Aldrich, St.Louis, MD, USA
Anti-rabbit IgG secondary antibody, goat	Invitrogen, Karlsruhe, Germany
GAPDH Monoclonal (6C5)	Thermo scientific

Cell Signaling
p44/42 MAPK (ERK1/2)
Phospho-p44/42 MAPK (ERK1/2)
(Thr202/Tyr204)
DakoCytomation
Polyclonal Anti-Mouse Immunoglobulins HRP
Polyclonal Anti-Rabbit Immunoglobulins HRP

4. Kits

Click-iT EdU cell proliferation kit	Thermo Fisher, Waltham, MA, USA

5. Buffers and solutions

Cell Lysis Buffer

- 30 mM TrisHCl (pH 8.0)
- 150 mM NaCl
- 1% Triton-X
- 10% Glycerol
- 1 tablet Protease inhibitor tablet

- 100 mM PMSF
- 0,5 M DTT
- 0,5 mM Sodium orthovanadate (Na_2VO_4)
- 500 mM Sodium Fluoride (NaF)
- 100 mM β-glycerophosphate

Tris-glycine –SDS Running Buffer 10X

- 14.4% glycine
- 3% Tris base
- 1% SDS
- pH 8.3-8.7

PBS-T Buffer 1X

- 50% 2XPBS
- 0.1% Tween 20

TBS-T Buffer 10X

- TBS
- 0.1% Tween 20

Blocking Solution

- 3-5% dry milk in ddH_2O

MTT-1 Solution

- 4 mM HCl
- 0.1% NP40
- Adjust with PBS

MTT-2 Solution

- 10% SDS
- 37% HCl

Freezing Medium

- 48.8% FCS
- 39% DMEM
- 12.2% DMSO

6. Chemicals reagents

Annexin binding buffer	Invitrogen,Karlsruhe,Germany
Annexin V	BD Biosciences, East Rutherford, NJ, USA
Amersham ECL Prime Western Blotting Detection Reagent	Marlborough,USA
Page Ruler Prestained Protein Ladder	Fermentas St. Leo-Rot, Germany

Merck, Darmstadt, Germany

Dimethylsulfoxid (DMSO), sterile

Ethanol

Methanol

Carl Roth, Karlsruhe, Germany

Dry milk powder

Magnesium chloride

Sodium dodecyl sulfate

Chloroform

Sigma-Aldrich, Steinheim, Germany

Tween 20

MTT formazan powder

Isopropyl alcohol

Triton X100

Propidium iodide (PI)

TRI Reagent RNA Isolation Reagent (TRIzol)

Crystal violet solution

Life Technologies, Carlsbad, California, USA

Hoechst 33342

Water (DNase/RNase-Free)

7. Equipment

Axiovert 40 Microscope	Carl Zeiss GmbH, Oberkochen, Germany
Heat block MR3001	Heidolph, Kehlheim, Germany
NanoDrop 1000 instrument	Thermo Scientific, Wilmington, USA
Shaker, Rock-N-Roller	G. Kisker, Steinfurt, Germany
Shaker, Unimax 1010	Heidolph, Schwabach, Germany
Water bath GFL1083	GFL, Wien, Austria
VortexGenie2	Scientific Industries, NY, USA
CO2-Incubator MCO-20AIC	Sanyo, Tokyo, Japan
Sunrise plate reader	Tecan, Männedorf, Switzerland

EVOS M7000 microscope	Invitrogen, Waltham, MA, USA
LSRFortessa cell analyzer	BD Biosciences, East Rutherford, NJ, USA
Imager	Raytest GmbH, Straubenhardt, Germany
2100 Bioanalyzer	Agilent Technologies, California, USA
Eppendorf, Hamburg, Germany	
Centrifuge 5702	
Heatblock Thermomixer comfort	
Bio-Rad, Munich, Germany	
Trans-Blot Turbo Transfer System	
Agarose gel electrophoreses apparatus	
Zeiss, Jena, Germany	
Axiovert 200M microscope	
AxioCam MRm	

8. Software

Connectivity map (build 02)	Lamb et al. 2007 [34], Qu and Rajpal 2012 [35]
ImageJ Software	NIH, Bethesda, MD, USA
GraphPad Prism 8	GraphPad, La Jolla, CA, USA
Office 2010	Microsoft, Washington USA
Chromas	Technelysium Pty Ltd, South Brisbane, Australia
Synergyfinder 2.0 software	Ianevski, Giri, et al. 2020 [38]
FlowJo software v10.4	BD Life Sciences
ShinyGO 0.76 package	Ge, Jung et al. 2020 [39]
STRING 11.5	Szklarczyk, Gable et al. 2021 [40]

Methods

1. Cell culture

Five conventional cell lines HUH6, HepG2, HepT1, Hep3B and HUH7 were grown in RPMI 1640 medium containing 10% (v/v) fetal bovine serum (FBS) and 1% Pen-Strep at 37°C in a humidified atmosphere with 5% CO2. We also cultivated other five cell lines named patient-derived xenograft (PDX) cell line in Advanced DMEM/F12 supplemented with 1% (v/v) penicillin-streptomycin, 1% (v/v) L-glutamine, 10% (v/v) fetal bovine serum (FBS)，and the Rho-associated kinase inhibitor (RKI) Y-27632 at 20μM final concentration.

2. MTT assay

We seeded the cells in 96-well plates at 1×10^4 cells/well in the culture medium, and the cells were treated the next day with DMSO or Mebendazole (MBZ) at 1:5 serial dilutions in the culture medium, and then cultured for 48 h at 37°C. MTT solution I was pipetted to each well, followed by incubation for 4 hours at 37°C. MTT Solution II was then added to each of the wells, followed by overnight incubation at 37°C. A Sunrise plate reader was used to measure sample absorbance at a wavelength of 595 nm. After the absorbance measurement, calculation of half-maximal inhibitory concentration (IC50) was performed with GraphPad Prism 8 software.

3. Wound healing assay

We seeded 0.5×10^6 cells/well at a density of 70%-80%. The confluent cell layer was scratched with a 100 μL sterile pipette tip, and cells were then synchronized in serum-free medium for 18 hours to prevent cell division. Medium containing DMSO (control) or MBZ (IC50) was changed after starvation. Then we took the images every 24 h using the Invitrogen EVOS M7000 microscope. The gap widths were assessed and quantified with the EVOS M7000 analysis software.

4. Proliferation assay

For the measurement of proliferation, we seeded cells at 1×10^5 cell/well into 24-well plates and cultured for 24 h before MBZ (IC50) and DMSO treatment. The Click-iT EdU cell proliferation kit has been tested as indicated. Briefly, we incubated cells with medium containing 100 μM ethynyl-deoxyuridine (EdU), the cells were treated with an appropriate concentration of MBZ and were incubated for 24 h at 37 °C. We then fixed the cells with 3.7 % formaldehyde for 15 minutes at room temperature, and rinsed the cells with 3 % BSA in PBS, permeabilized the cells with 500 μl of 0.5 % Triton-X100 for 20 minutes at room temperature and rinsed again with 3 % BSA in PBS. Cells were then stained with Click-iT reaction cocktail, washed with 3% BSA in PBS and counterstained with Hoechst 3333342 staining diluent for 30 minutes in the dark at room temperature. After removal of the staining solution, samples were imaged containing PBS using an Invitrogen EVOS M7000 microscope.

5. Colony formation assay

We seeded 1×10^4 cells in per 6-well plate. The next day, the cells were treated with 0.5 µM MBZ and then cultivated for 5 days. The cells were then fixed with cold methanol for 15 minutes and stained with 0.5% crystal violet solution for 1 h. Images were captured using an Invitrogen EVOS M7000 microscope. Colonies were counted using ImageJ software to determine the number of colonies.

6. Spheroid formation assay

To get the cell spheroids, we cultured 1×10^3 cells in 96-well round-bottom plates with very low fixation to form pellets for 7 days, and then the cells were treated with different concentrations of MBZ. Images were taken on days 0, 4 and 7 after treatment using an Invitrogen EVOS M7000 microscope. The volume of the spheroids was calculated as follows: $V\ (\mu m^3) = [(\text{length}\ (\mu m)\ \text{x width}\ (\mu m)^2) / 2]$ as previously described [41].

7. Cell cycle analysis

Cells were grown in serum-free medium for 24 h to synchronise. After 48 hours of treatment with MBZ or control, modified Advanced DMEM/F12 medium containing 1 µg/ml Hoechst 33342 was added to stain the cells for 30 minutes in the dark at 37°C. Cell phase distribution was determined by flow cytometry on an LSRFortessa cell analyser, and data were analysed using FlowJo v10.4 software.

8. Immunofluorescence

2×10^5 cells were seeded on 8-well chambered coverslips and treated with DMSO and MBZ for 24 hours. Cells were then fixed in 4% paraformaldehyde/PBS for 15 minutes, permeabilised with Triton X-100 for 1 hour and blocked in PBST with 3% BSA and 0.1% glycine for 10 minutes. Primary anti-α-tubulin antibody was added with 5% BSA/PBS in a humidified chamber at 4°C overnight. Polyclonal goat anti-mouse/HRP immunoglobulin with 5% BSA and 0.1% Triton X-100 and 1 µg/ml Hoechst 33342 was added at room temperature for 1 hour in the dark. Images were acquired using an AxioCam MRm and AxioVision software loaded on the Axiovert 200M microscope. Spindle counts were performed with ImageJ and calculated with GraphPad Prism 8 software.

9. Apoptosis assay

The measurement of apoptotic cells exposed to MBZ or control vehicle for 48 hours was performed by cytometry. Medium and trypsinised cells were collected in tubes, rinsed twice with PBS and resuspended in binding buffer. The cells were stained twice with APC-conjugated Annexin V 1:20 and propidium iodide 20 ng/ml. Cells were harvested by flow cytometry on a BD LSRFortessa cell analyser, and the percentage of cells undergoing apoptosis was determined using FlowJo v10.4 analysis software.

10. RNA sequencing

The cells were seeded in 6-well plates and exposed to MBZ (IC50) and DMSO (control) for a period of 24 hours. TRIzol, as recommended by the supplier, was used to isolate total RNA from the cell lines.
The quantification and quality control of the RNA samples were carried out using a Nanodrop ND-1000 and a 2100 Bioanalyzer, respectively. Library preparation from 2 µg total RNA using the TruSeq stranded mRNA kit and sequencing on a HiSeq2500 system as 100 bp paired-end runs, as well as all subsequent steps, were performed by the Helmholtz Core Facility Munich. The known genes of the human genome combination HG19 (GRCh37) and UCSC were compared using the STAR aligner V2.4.2A with modified parameter settings (--two-passMode=Basic). Annotated gene read counts were quantified using HTseq-count V0.6.0. Bioconductor's DESeq2 package was used to normalise data for differential gene expression between treated and untreated cell lines. Gene enrichment analysis was performed using the ShinyGO 0.76 package. Differentially expressed genes >2-fold with $p < 0.5$ were used as inputs. Results were ranked and sorted by fold enrichment according to the false discovery rate, which is based on the nominal P-values of the hypergeometric test.

11. Western blot

HB cells were seeded in 100 mm Petri dishes at a density of 3×10^7 cells per plate, allowed to adhere overnight and treated with MBZ for 24 h. Lysates of all cells were prepared in cell lysis buffer modified with ERK1/2 protein and phosphorylated ERK protein, then centrifuged at 13,000 g for 30 min at 4°C.We separated 25 µg of total cell lysate on 3-8 % SDS-acrylamide gels, and then transferred the separation to a PVDF diaphragm. The diaphragms were incubated with p44/42 MAPK (ERK1/2) antibody, phospho-p44/42 MAPK (ERK1/2) antibody (Thr202/Tyr204), monoclonal GAPDH antibody (6C5), polyclonal anti-mouse HRP and polyclonal anti-rabbit HRP immunoglobulin. The signal was detected using Amersham ECL Prime Western Blotting detection reagent and captured using ImageJ.

12. Synergy assay

100,000 cells were seeded in 96-well microtiter plates, and 20 µl of combinations of either MBZ together with cisplatin or cisplatin and doxorubicin in concentrations of 1–100 nM were added into the all the wells and cultured for 48 h. Viability was measured by MTT assay as described above. Synergy scores were determined using the SynergyFinder 2.0 software that exploits the HSA calculation method. The maximum synergy score was calculated, and concentrations for the maximum synergy were noted [38]. Data visualization and statistical testing were performed using Prism 8.

13. Animal studies

In accordance with the authorisation for vertebrate animal experiments granted by the French Ministry of Higher Education, Research and Innovation (APAFIS#29136-2020121415204532, 15 January 2021),

XenTech performed animal studies as previously described [42]. Briefly, five-week-old female nude Foxn1nu mice were implanted in the interscapular region by cryopreserved tumour fragments of the HB-282 PDX model. We maintained the same mean and central volume of the tumour in each arm, mice with subcutaneous tumours ranging from 75 to 288 mm^3 were divided into two groups after a lag period. Mice were treated orally with 40 mg/kg MBZ suspension in PBS for 5 days, then stopped for 2 days. The measurement of the length and width (determined by the longest and shortest diameters of the tumour) with a caliper was assessed three times per week during the course of latency and treatment. The formula used to determine tumour volume (TV) was TV (mm^3) = [(length (mm) x width $(mm)^2$) / 2]. All animals were weighed at the time of tumour measurement, and changes in behaviour, appearance and clinical condition were daily monitored. At each time point, the ratio of the mean TV of the MBZ-treated group to the control group was computed.

14. Statistical analysis

Data are presented as mean ± standard deviation (SD) or mean ± standard error of the mean (SEM). In all analyses, differences between two groups were analysed by Student's t-test and differences between multiple groups by two-way ANOVA. Gene pathway enrichment and biological processes in the hypoxia-inducible gene ontology were analysed using the Enrichr web server (http://amp.pharm.mssm.edu/Enrichr). The significance criteria for all comparisons were $p < 0.05$ (significant) and $p < 0.01$ (highly significant).

Results

1. The identification of MBZ as a candidate drug for HB

To investigate potential chemotherapy options for HB, we used the bioinformatics tool Connectivity Map (CMap) [34] and RNA sequencing dataset in patients with HB for whom data on the response to therapy were available. We distinguished responder and non-responder according to the level of AFP, which comes from the HB 99 Germany protocol after two cycles of chemotherapy [43]. We defined the >10-times decrease of AFP level as responder after treatment, while the decrease of AFP level as less than 10-times, or no response as non-responder after treatment (**Figure 1**). We selected 273 up-regulated and 458 down-regulated genes (see Supplementary Table S1 for top 50 genes by fold change) out by comparing the expression levels of 2 non-responders with 5 responders. These genes differentially expressed became a genetic signature, which was put to CMAP for the identification of compounds with negative correlation values, suggesting a possibe application in patients with chemoresistant HB. Among 23 compounds found in CMap, there were two drugs, namely sirolimus and LY-294002 that have been confirmed in HB before [44][45]. The Connectivity score of mebendazole (MBZ) was lower than the ones seen for the two other drugs, which means that MBZ is a promising drug for HB patients.

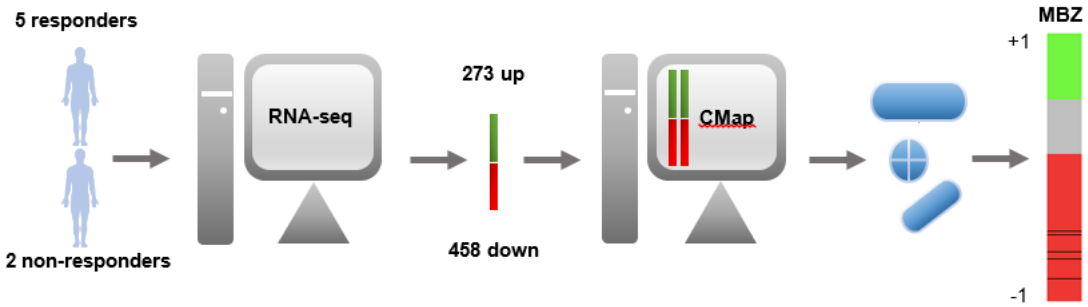

Figure 1. Drug identification.
RNA sequencing data of 5 responders and 2 non-responder patients was queried in Connectivity Map to do drug repurposing. The connectivity score of potentially effective drugs for HB is shown.

2. MBZ inhibits pediatric liver cancer cells viability

For tumour growth and other malignant behaviour, cell viability is a prerequisite. As previously reported in different types of cancers other than HB, MBZ treatment impairs cell proliferation ability and induces cell apoptosis via different signaling pathways [46].

To determine whether MBZ treatment regulates HB cell viability, we dynamically monitored the growth of HB cells exposed to different concentrations of MBZ solution from 0.00128 μM to 20 μM by MTT assay.

There was a decrease in cell viability as the concentration of MBZ increased, showing significantly impaired cell viability under MBZ treatment (**Figure 2**). As most liver cancer cell lines were sensitive to MBZ, we selected PDX cell lines HB-214, HB-282, and HB-303, being the most sensitive ones as our experimental validation cell lines.

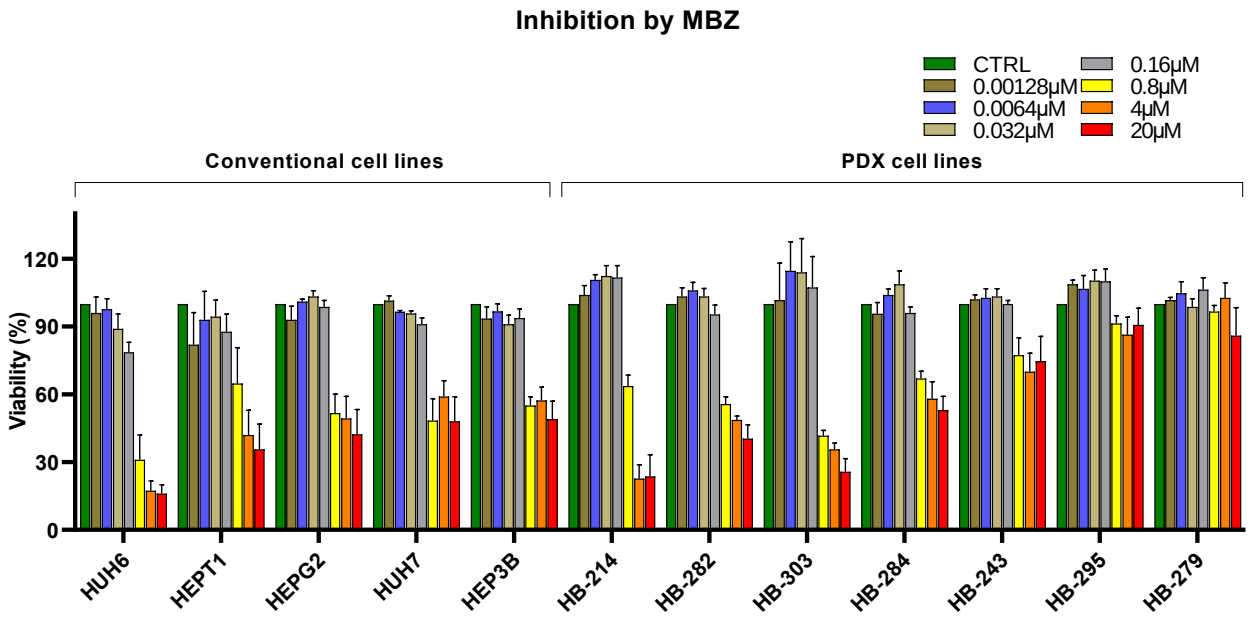

Figure 2. Cell viability after MBZ treatment at various concentrations.
Cell viability after 48 hours of treatment with MBZ and DMSO as a control. Bars represent the mean ± SEM error of three independent experiments, calculated as the average of 4 duplicates.

3. MBZ decreases migration of HB cells

We next analyzed the effect of MBZ treatment at the previously determined IC50 on HB cell migration and invasion by observing the time required for the cells to close the gap formed by scraping the liquid cell layer. We found that MBZ treatment reduced HB cell migration (**Figure 3**) by about twofold during gap closure. Therefore, these data suggest that MBZ affects cell growth by affecting migration.

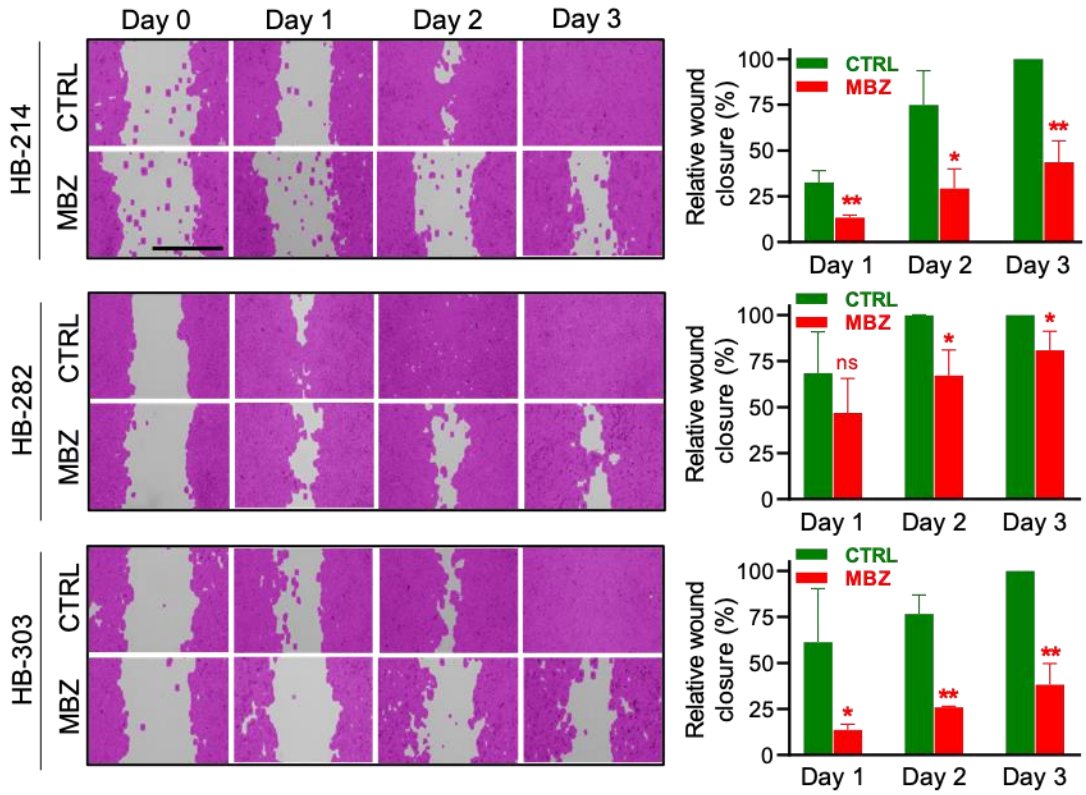

Figure 3. MBZ (mebendazole) inhibited invasion.
The cells were synchronised with serum-free medium for a period of 18 hours, then treated with CTRL (controll) and MBZ in IC50, which respectly are 2 μM, 4 μM, and 2 μM after 1 day, 2 days, and 3 days in wound healing assay of one experiment in triplicate. Scale bar ＝300 μm. Bars represent the mean ± standard error of the mean. Ns = not significant, *$p < 0.05$, **$p < 0.01$ compared to CTRL by Student's t-test.

4. MBZ inhibits HB cell short-term proliferation

To investigate whether MBZ treatment would inhibit the proliferation ability of HB cells in short-term, cells were monitored in a plate proliferation experiment. Fluorescence microscopy analysis of Click-it EdU kit stained cells was undertaken to study proliferation and nuclear alterations. HB cells treated with MBZ exhibited a decrease in proliferating cells dramatically in HB cells under investigation (**Figure 4**). We can intuitively see that MBZ inhibits the proliferation of HB cells in the short term.

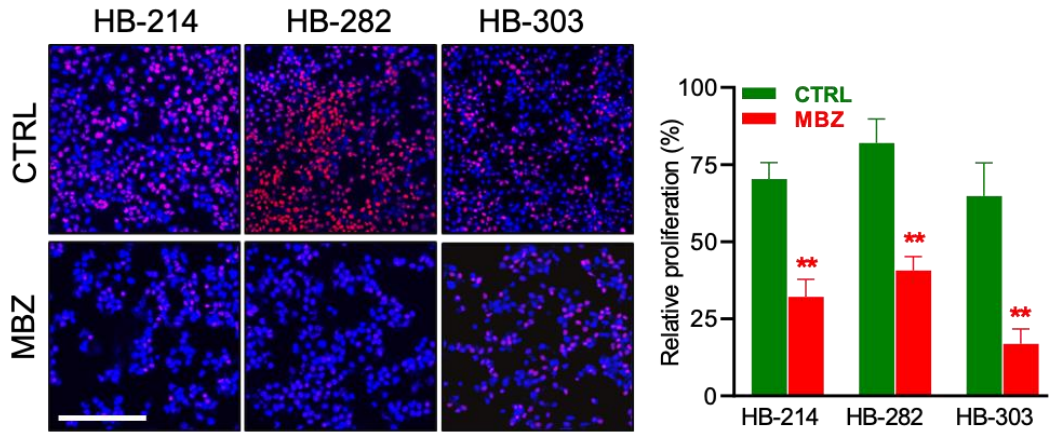

Figure 4. MBZ significantly inhibited proliferation.
Cells were treated with CTRL (DMSO) and MBZ in IC50 (2 μM, 4 μM, and 2 μM) and stained with EdU and Hoechst staining after 24h in proliferation assay of one experiment in triplicate. Scale bar＝300 μm. The bars represent the mean ± standard d error of the mean. ** $p < 0.01$ compared with CTRL (DMSO) student's t-test. Pictures modified from Li, Qian, et al. [47]

5. MBZ inhibits HB cell long-term proliferation

We also wanted to investigate the colony-forming ability of cells in long run. After 5 days of treatment of MBZ and DMSO, very few colonies formed of these three HB cell lines, respectively, significantly compared with the DMSO group (0 vs 10.8,0 vs 10.5,0 vs 9) (**Figure 5A**, $p < 0.05$). The data showed that treating HB cells with MBZ inhibited the ability to colonise.

MBZ's inhibitory effect on HB cell growth was tested by spheroid formation assays, which also means long-term proliferation, showed that MBZ treatment severely impacted the sphere-forming ability of HB cells, triggering about the threefold decrease in sphere volume (**Figure 5B**).

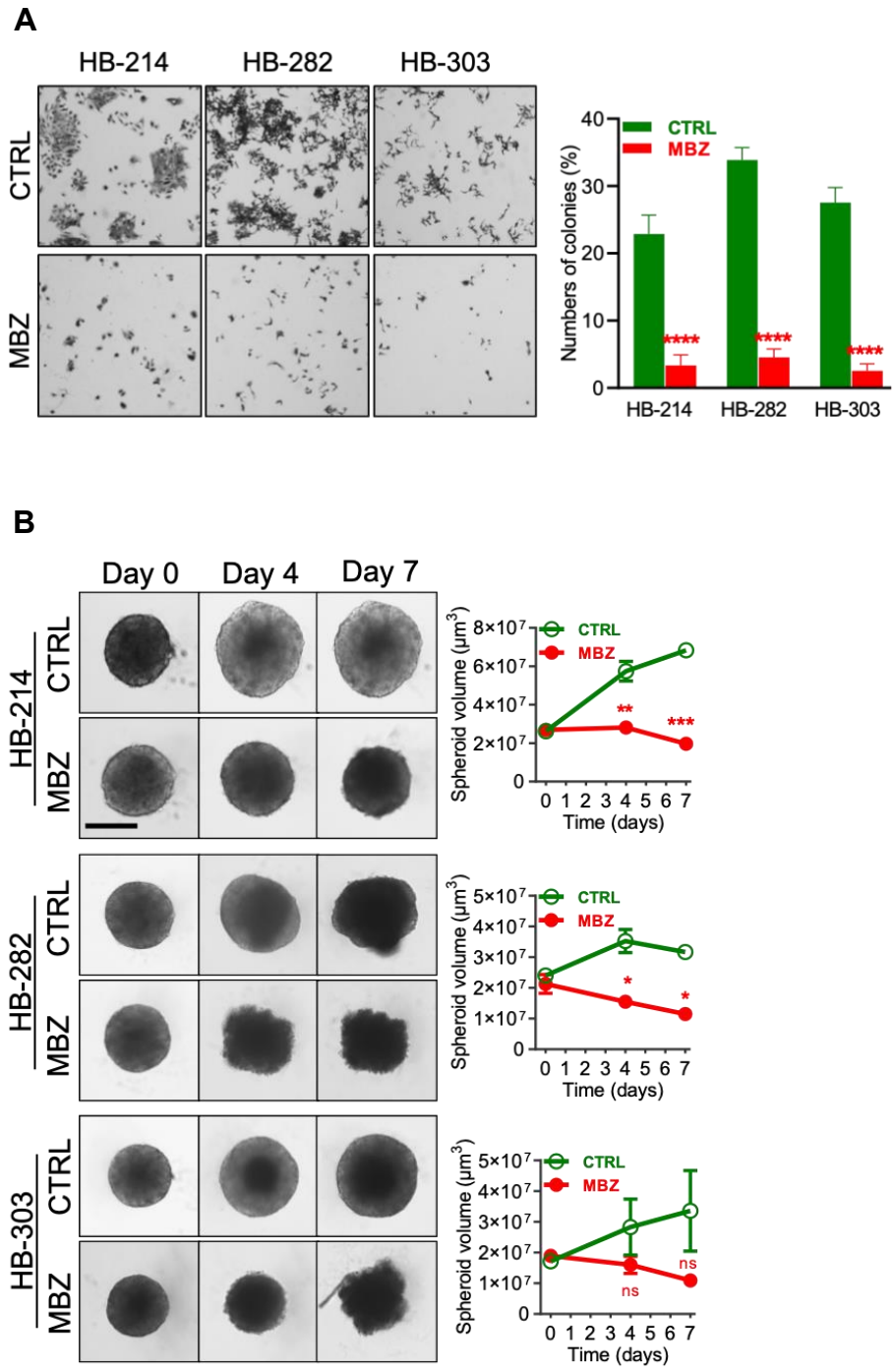

Figure 5. MBZ inhibits long-term cell proliferation.
A) Cell were treated for 24 h with CTRL and 0,5 µM MBZ after 5 days treatment of one experiment in 9 duplicates. Scale bar ＝750 µm. **B)** Cells were seeded containing DMSO and MBZ for 4 days of one experiment in triplicate in spheroid formation assay. Photos were taken on day 4 after treatment. Scale bar ＝300 µm. The bars represent the mean ± standard error of the mean. ** $p < 0.01$, **** $p < 0.0001$ compared with CTRL (DMSO) by Student's t-test. Pictures modified from Li, Qian, et al. [47].

6. MBZ reduces the growth of spheroid

We further confirmed the effect of MBZ in a patient-near condition, namely 3-dimensional spheroids. Established spheroids in the control group continued to grow, while the spheroids after MBZ treatment did not continue to grow, with the change in the shape of the sphere (**Figure 6**). MBZ not only inhibits the growth of the spheroids, but also reduces the volume of the spheroids.

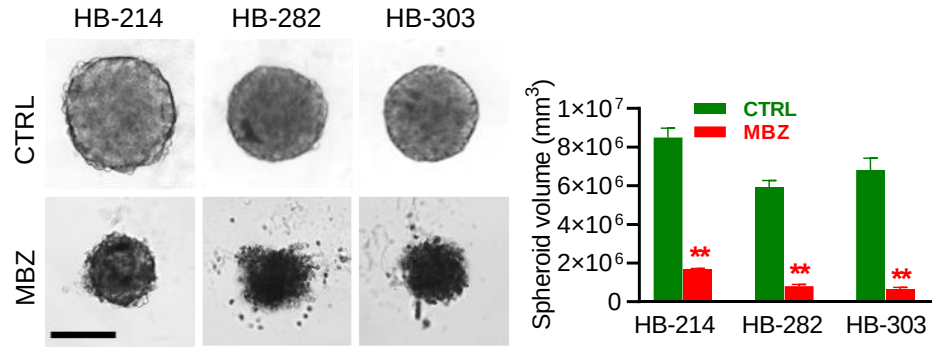

Figure 6. MBZ reduces the growth of spheroid.
Tumour spheroids were generated by culturing cells for 7 days. Cells were then exposed to CTRL and MBZ at IC50 (2 μM, 4 μM, and 2 μM) for 4 days in spheroid volume assay of one experiment in triplicate. The photos were taken on the 0th day, the 4th day and the 7th day after the treatment. The bars represent the mean ± standard error of the mean. Ns = not significant, *$p < 0.05$, **$p < 0.01$, ***$p < 0.001$ compared with CTRL (DMSO) by Student's t-test. Pictures modified from Li, Qian, et al. [47].

7. MBZ disrupts spindle formation

To study the effect of MBZ treatment on HB cell mitosis, immunofluorescence was performed to observe the formation of spindles of HB cells MBZ or DMSO (Control) treatment for 24 hours. We observed that microtubules disarrayed, and a significantly higher percentage of abnormal spindles formed in MBZ-treated HB cells than in the control (0% vs 11.5%, 0% vs 7.8%,0% vs 20%, $p<0.05$) (**Figure 7**). This means that MBZ can affect the process of chromosome segregation.

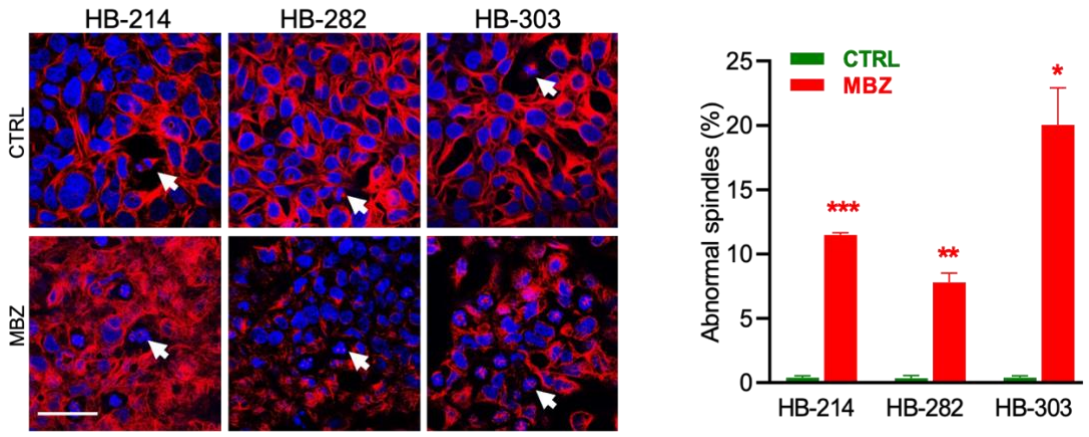

Figure 7. MBZ induces disarrayed microtubules and abnormal spindles.
HB-214, HB-282 and HB-303 cells were incubated with vehicle or MBZ at IC50 (2 μM, 4 μM and 2 μM, respectively) for 24 hours, then were fixed and stained with α-tubulin (red) antibody and DAPI (blue) in two independent experiments in 10 duplicates. Normal and abnormal spindles were shown with arrows in CTRL and the treated group, respectively. The bars represent the mean ± standard error of the mean. *$p < 0.05$, **$p < 0.01$, ***$p < 0.001$ compared with CTRL (DMSO) by Student's t-test. Pictures modified from Li, Qian, et al. [47].

8. MBZ induces G2/M arrest in the cell cycle

It is known that microtubule-targeting agents can cause cell cycle arrest in the G2/M phase in cancer cells [48]. To verify this, Flow cytometry was used to determine the effect of MBZ treatment on the induction of cell cycle arrest in HB cells. After 48 h of exposure to MBZ treatment at 2 μM, 1 μM, and 2 μM, the percentage of G2/M phase cells increased by MBZ treatment as compared to control (**Figure 8**). The results showed that MBZ treatment disrupts spindle formation and causes mitotic arrest.

This can explain the above finding, because of the disorder of microtubules, the abnormality of the spindle, cells are arrested in the G2/M phase, so cells no longer continue to divide, and then no longer grow.

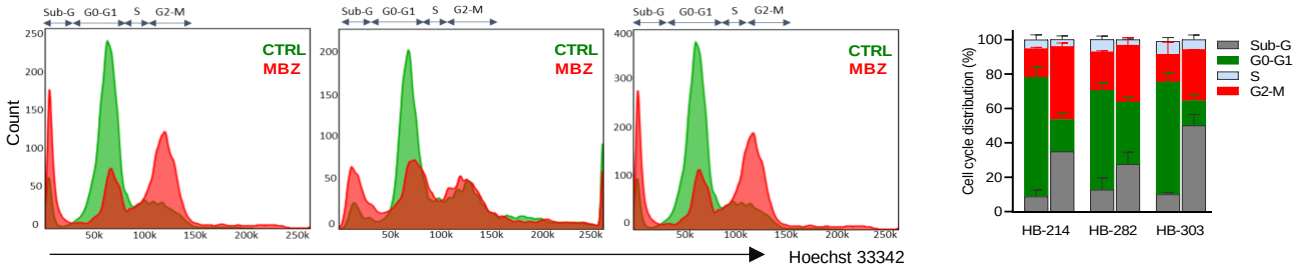

Figure 8. MBZ induces G2/M arrest in the cell cycle.
After 24 h synchronizion with serum-free medium, cells were treated with 2 μM, 1 μM, and 2 μM MBZ for 48 h after being stained with Hoechst 33342 in two independent experiments. Cell cycle phase distribution

was analyzed by flow cytometry. The bars represent the mean ± standard error of the mean. Pictures modified from Li, Qian, et al. [47].

9. MBZ induces HB cell apoptosis

The effect of MBZ treatment on HB cell apoptosis was then determined by Annexin V/PI double staining and flow cytometric analysis. (**Figure 9**). The results showed that the MBZ treatment ultimately led to apoptosis. HB-303 cells were more sensitive to MBZ treatment, with higher levels of apoptosis observed compared to HB-214 and HB-282 cells.

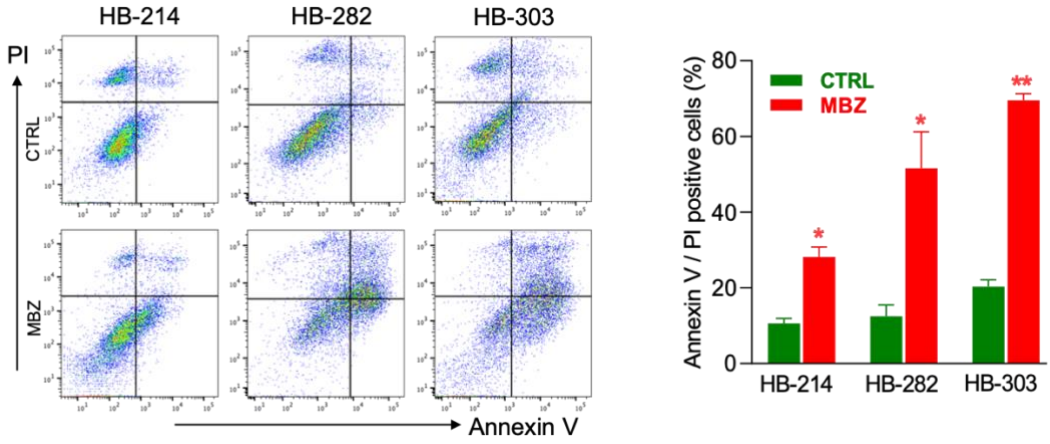

Figure 9. MBZ induces HB cell apoptosis.
Measurements of apoptotic cells were performed on HB-214, HB-282, and HB-303 exposed to 2 µM, 4 µM, 2 µM MBZ, or vehicle control for 48 h after Annexin V and propidium iodide double staining in two independent experiments. The bars represent the mean ± standard error of the mean. *$p < 0.05$, **$p < 0.01$ compared with CTRL (DMSO) by Student's t-test. Pictures modified from Li, Qian, et al. [47].

10. MBZ is involved in dysregulation of gene expression associated with cell growth and cell cycle regulation

To obtain a broader view of the relevance of MBZ treatment in the transcription response to treatment, HB-214, HB-282 and HB-303 cells were subjected to MBZ treatment at IC50 for 24 hours and RNA was isolated for high throughput RNA sequencing.

By comparing the expression values of the three MBZ-treated against the 3 control-treated cell lines we were able to detect 273 genes up-regulated and 458 genes down-regulated. By analysing these genes, we found that that spindle formation-related genes, Histone related genes (such as HIST1H2AC) were upregulated, and microtubules related genes (like TUBB, TUAA1B, and TUBB4B) were downregulated (**Figure 10A**), which were consistent with the ability of MBZ treatment to interrupt microtubules, the formation of spindles during HB cell mitosis. That further confirmed that MBZ is a microtubule inhibitor and damages DNA replication.

The analysis of differentially expressed genes in Gene Ontology (GO) enrichment showed that the category 'repair of double-strand breaks by replication' was the most enriched, with 'cell cycle and apoptosis' also in the top 20 categories. Pathway enrichment analysis also demonstrated that the 'MAPK cascade pathway' was a significantly enriched category (**Figure 10B**).

Cell apoptosis was another category identified by pathway enrichment analysis. It has been described that apoptotic stimuli could be mediated by the MAPK signaling pathway [49]. Activation of the pathway was demonstrated by phosphorylation of specific tyrosine (Tyr) residues of ERK using immunoblot assays, which showed that phosphorylation of ERK was increased in response to MBZ treatment of HB cells, particularly in HB-282 cells. However, there was no change to the total ERK protein level (**Figure 10C**), indicating that the p-ERK pathway was activated in these HB cells treated with MBZ.

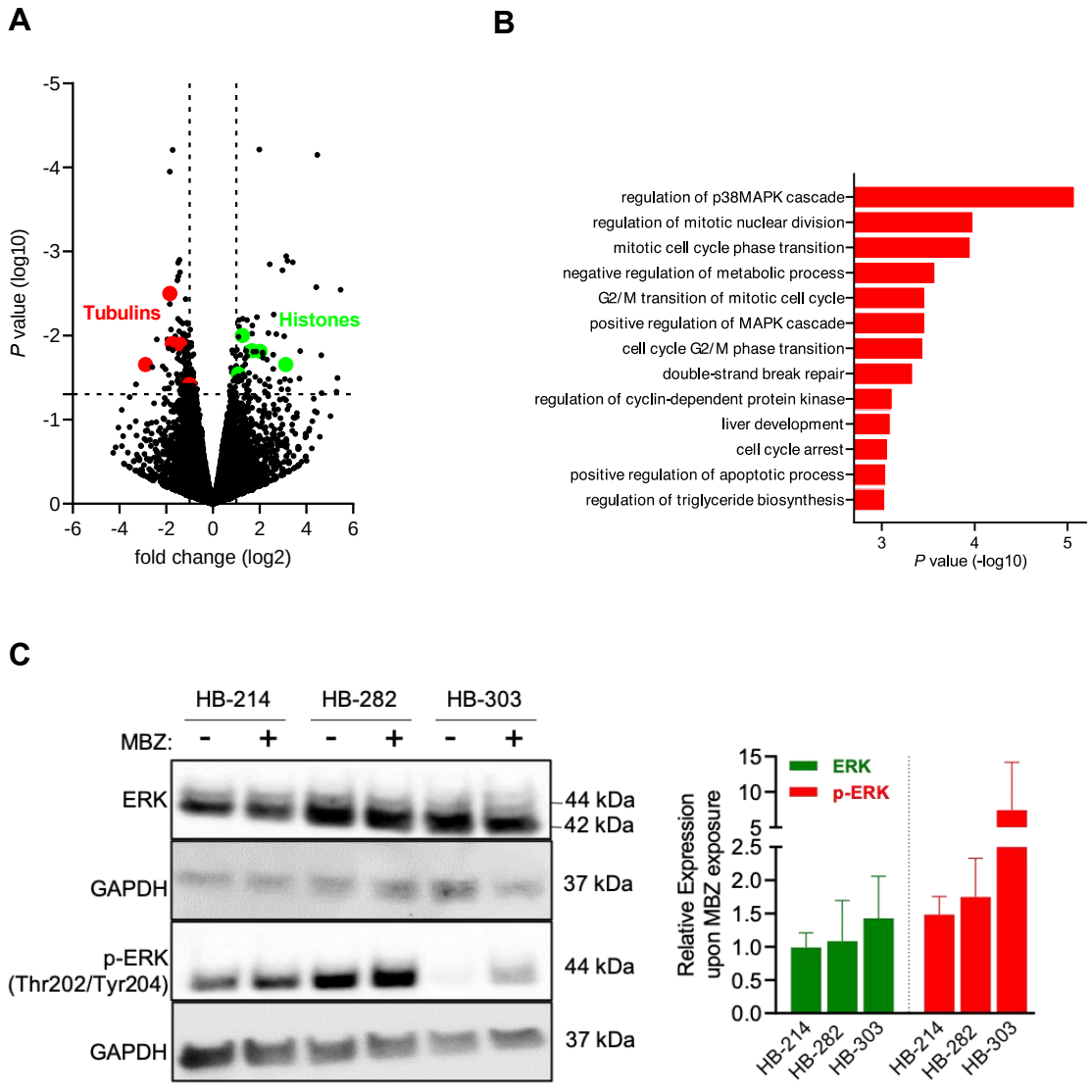

Figure 10. MBZ is involved in dysregulation of gene expression associated with cell growth and cell cycle regulation.

A) Volcano plot displaying differentially expressed genes between MBZ-treated and control-treated HB-214, HB-282, and HB-303 cells, as determined by RNA sequencing. Green dots represent up-regulated genes (log2 fold change＞1). Red dots represent down-regulated (log2 fold change＜1). **B)** Gene ontology analysis was carried out on differentially expressed genes. $p < 0.05$ displaying enrichment in cellular pathways. **C)** MBZ induces ERK phosphorylation. HB-214, HB-303, and HB-282 cells were treated with MBZ IC50 (2 μM, 4 μM, and 2 μM) for 24 h in three independent experiments and analyzed by Western blotting to determine the phosphorylation of ERK and p-ERK1/2 (Thr202/Tyr204). GAPDH was used as a loading control for the assay. The bars represent the mean ± SEM error of the mean of triplicate independent experiments. Pictures modified from Li, Qian, et al. [47].

11. MBZ combined with cisplatin exhibited synergistic activity in HB cells

Cisplatin and doxorubicin are cytotoxic drugs that damage DNA and are used as standard chemotherapy for patients who have been diagnosed as having HB, but can often develop drug resistance. We therefore wanted to test whether there was a potential synergistic effect in targeting HB cells when cisplatin is combined with MBZ.

Cell viability assays were first used to determine the potential synergy of the combination of MBZ and cisplatin. Cell viability values were used for the calculation of drug synergy in the highest single agent (HSA) model with the SynergyFinder 2.0 tool [38]. All three HB cell lines tested showed synergistic activity in this assay. (**Figure 11**). The results showed a higher maximum synergy score (MSS) in HB cells treated with MBZ and cisplatin combination than that in HB cells treated with doxorubicin and cisplatin combinations (MSS 29.7 vs 24.86 in HB-214 cells, MSS 47.56 vs 24.17 in HB-282 cells, and MSS 41.34 vs 32.87 in HB-303 cells), indicating combining MBZ with cisplatin may be a better choice when treating patients diagnosed with HB, especially for chemoresistant patients.

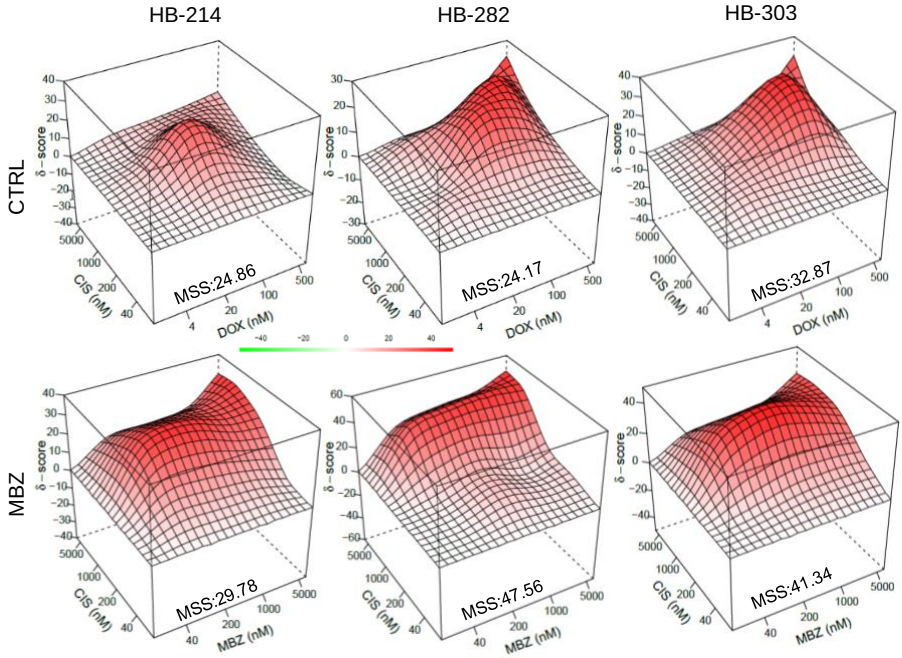

Figure 11. MBZ in combination with the standard of care treatment.
4 increasing concentrations for each compound in a combination matrix from MTT assays with duplicates. Synergy finder 2.0 software was applied to calculate Maximum synergy scores (MSS) with the HSA model. Pictures modified from Li, Qian, et al. [47].

12. MBZ inhibits tumour growth of HB cells in a mouse model

To more directly verify the impact of MBZ in the near-patient environment, an *in vivo* experiment proceeded. We transplanted cryopreserved tumour specimens of the PDX model HB-282 into nude-Foxn1nu mice and let them grow for 3 weeks. Mice with manifested tumours were then orally treated either with MBZ or vehicle (**Figure 13A**). In comparison with tumours in vehicle-treated mice for 2 weeks, tumours in mice treated with MBZ showed a significantly decreased volume (**Figure 13B**), and the final mice weights did not change compared to the vehicle-treated group (**Figure 13B**).

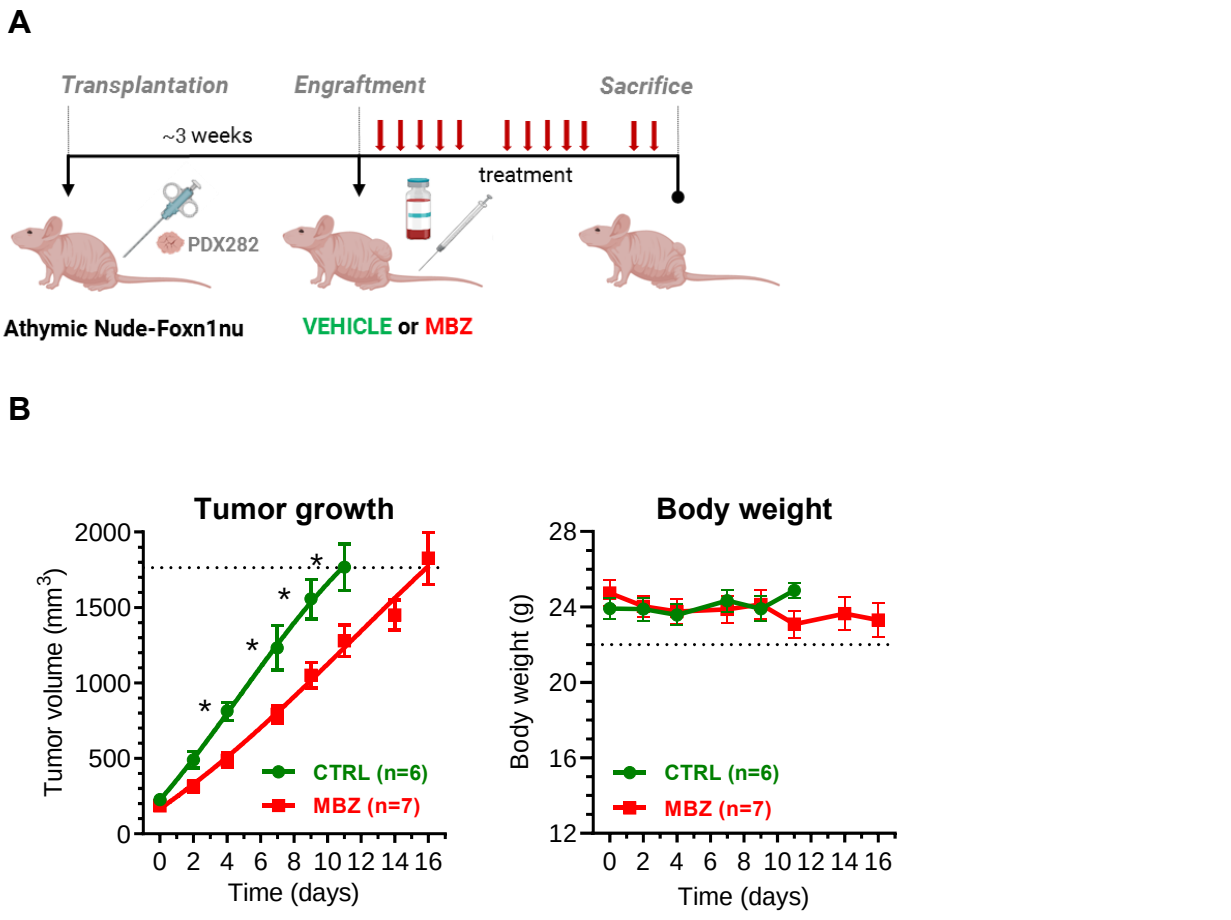

Figure 12. MBZ inhibits tumour growth *in vivo*.
Experimental overview of how MBZ gets tested *in vivo*. **A)** Mice were implanted with HB-282 tumours for 3 weeks. They were then treated with MBZ (40 mg/kg body weight) or vehicle (CTRL) by oral gavage 5 times per week. They were sacrificed when they reached the maximum tolerated tumour size of 1,764 mm3. **B)** The changes of tumour growth (left panel) and body weight (right panel) treated with either MBZ (n = 7) or vehicle (n = 6) in mice. Figures represent average tumour volumes and average body weights

±SEM. Maximum allowable values are indicated by dashed lines. Pictures modified from Li, Qian, et al. [47].

Discussion

Adding to the difficulty of improvement in survival of children with HB, the safety management of long-term and continuous infusion of doxorubicin or cisplatin is still challenging. Especially for children with disease that is inoperable or metastatic, the 5-year survival rate is far less than those who are eligible for radical resection or orthotopic liver transplantation [50][51][52]. From the perspective of unmet medical needs, compared to conventional chemotherapeutic agents， approved drugs repurposed for pediatric cancers may provide a promising strategy with a lower level of safety concerns.

In this study, we hoped to identify new drugs by comparing the differential gene expression of HB patients with those of cancer cell lines treated with 1,309 FDA-approved small molecule drugs, which are contained in the CMap platform [33]. According to the definition of the German HB99 protocol [43], we differentiated responder and non-responder patients by the level of AFP changes after the classical treatment regimen. By introducing significantly high and low expressed genes selected from RNA sequencing data of non-responders into CMap, we were able to identify several drugs putatively active against chemoresistant tumours, of which MBZ ranked very high by its connectivity score.
MBZ is commonly prescribed for the treatment of a wide range of infections caused by parasitic worms. and has a very well safety profile. It can be used for children over 2 years old. There are also many reports that it can be used for children under 2 years old, and even newborns [53][54]. The side effects are very small and the symptoms are reversible, especially the price is affordable, and it is very suitable for children. The anti-tumour effect of MBZ has been validated for the treatment of several forms of cancers including both preclinical and clinical settings [55][56], which support the application of MBZ in HB.

The main anti-parasitic effect of MBZ is because it acts as a microtubule-disrupting agent, preventing the polymerization of tubulin in helminths' guts, which kills the parasites [57]. Paclitaxel, colchicine, and vincristine are a few regularly used chemotherapeutic medicines that target tubulin since it is essential for cell division [58][59]. Like the other benzimidazoles, MBZ binds to the tubulin's colchicine-binding domain [60]. A glioblastoma model [61] and a melanoma model [62] have both provided *in vitro* confirmation of the suppression of tubulin polymerization by MBZ. But with HB, this has not yet been verified before.

To best simulate the actual response of HB to MBZ treatment, we used conventional cancer cells, especially also PDX-generated HB cells from three patients in this work. A variety of patient-derived models that more closely resemble the *in vivo* tumour than immortalized cancer cell lines are necessary for the development of tailored therapeutics. Primary tumour cells isolated from patient tissue that have been cultivated in a short-term culture can produce high-fidelity information that can be used to translate *in vitro* results to *in vivo* models and, ultimately, to therapeutic settings. Compared to immortalized cells or tissue banks, which can dramatically diverge from the original patient's disease, this offers more precise data sets.

After the selection of cell lines, we validated the new target drug MBZ and proceeded with a series of cellular experiments on conventional cancer and PDX cell lines mentioned above and found that most of these cell

lines are sensitive to MBZ. We show that MBZ treatment dramatically impairs the ability of PDX-derived HB cells to proliferate and to migrate. Since MBZ is already confirmed as one microtubule inhibitor, inhibitors targeting mitosis usually disrupt microtubule polymerisation to prevent cells from dividing [63], thus preventing cancerous growth. Microtubules created by polymerizing tubulin components are long polymers made of monomers of the protein tubulin [64], moving, separating chromosomes, and other cell components for cell division. Mitotic inhibitors inhibit the assembly and disassembly of tubulin into microtubule polymers, thereby preventing mitosis [65], thus halting cell division, which typically occurs in the cell cycle's mitotic (M) phase [66]. In cell division, spindle is an essential part of mitosis, its main role has two parts. One is the arrangement and division of chromosomes. The integrity of the spindle determines the correctness of chromosome division. The normal generation of the spindle is necessary for the arrangement of chromosomes [67]. Another function of the spindle is to determine the division plane of cytokinesis [68]. MBZ treatment blocks HB cells from dividing and by interrupting the construction of the microtubules network and spindle formation shown by immunofluorescence assays, suggesting targeting microtubules and spindle network, then causing cell cycle arrest at the G2/M phase, might be the underlying mechanism paving the way for MBZ treatment induced cell apoptosis.

Further, we performed immunoblots to confirm the possible molecular mechanism of such effects of MBZ on HB cells. We found MAPK/ERK pathway is quite correlated with MBZ. ERK is rapid and transient, occurring within minutes or hours of treatment [69], and its activation is closely related to apoptosis induction [70]. We captured that the expression of phosphorylated ERK protein was significantly upregulated as compared with control after treatment for 24 h, indicating the MBZ might participate in the MAPK/ERK pathway. In other reports, we found the same patterns that doxorubicin, quercetin [71], and paclitaxel [72] initiate apoptosis rather than promoting survival with different time treatments. Above all, we concluded that MBZ activates the MAPK/ERK signaling pathway in HB cells. We have shown for the first time that there is a close connection between ERK activation and MBZ-induced apoptosis in HB cells. ERK pathway might be one of the underlying mechanisms contributing to MBZ treatment. Whether this pathway plays an essential function in HB cells needs to be investigated further.

In addition, to investigate the effects of MBZ treatment on PDX-derived HB cells, we also explored the potential molecular mechanisms governing the cell growth inhibition by MBZ and increased cell apoptosis and cell cycle arrest by RNA sequencing. A significant number of genes whose expression is regulated in relation to MBZ treatment were identified by RNA-seq analysis. As expected, we identified the differential expression of genes encoding factors that play important roles in spindle formation [73], microtubule construction [74], and cell cycle regulation [75]. Moreover, unexpectedly, a set of genes induced by MBZ treatment in HB cells was identified by gene ontology analysis and encoded proteins involved in DNA unwinding during replication, with “double-strand break repair via break-induced replication” ranking in the top significantly enriched category. The results of RNA sequencing are consistent with previous reports and our speculation that MBZ not only induces disturbance of the microtubule system, resulting in a significant down-regulation of tubulin genes, but also affects DNA replication by participating in the up-regulation of

unwindosome genes. This finding suggests that MBZ may hinder HB cells to complete mitosis and further proliferation, and in the end, induce apoptosis.

The conventional treatment regimen has its limitation, that is, some patients are not sensitive to cisplatin and need to be supplemented with doxorubicin with stronger drug efficacy. The combined drug effect is better, but doxorubicin has strong drug side effects. We combined cisplatin with the newly discovered MBZ, compared the conventional regimen of cisplatin and doxorubicin, and found that MBZ can be used as a very safe alternative to doxorubicin, even in the case of high-dose medication.

In order to study the performance of MBZ in a patient-near environment, we conducted mouse experiments. We found that growth of tumour cells in the mice was dramatically reduced after MBZ treatment for two weeks, and the body weight remained unchanged, which further fully demonstrated that MBZ inhibits the growth of tumour cells with considerable inhibitory effect.

Thus, MBZ is a repurposed, FDA-approved drug with a known toxicity profile, such that it can be more easily adapted to clinical trials with less risk than a newly developed drug. The evidence presented here on the use of preclinical HB cell models in combination with the safety of high doses of orally administered MBZ suggests a clinical trial against these cancers.

Summary

HB is a rare childhood disease with a low reported incidence and rarely gets noticed, especially for those children who are resistant to conventional chemotherapy, the development of new drugs is imminent. The purpose of our project is to find new, affordable, effective, and safe treatments for HB patients.
Through the drug prediction CMap tool, we found an FDA-approved drug, MBZ, which is an antiparasitic drug recommended by the WHO. We further studied the mechanism of MBZ at the cellular level, gene expression, and protein expression level, and also combine it with cisplatin to compare the standard of care regimen. We found that MBZ inhibits short- and long-term cell proliferation, is synergistic in combination with cisplatin, impairs sphere formation and induces G2/M arrest, disrupts spindle formation, induces apoptosis, downregulates DNA replication-associated genes, and reduces the growth of patient-near spheroid and xenograft models. Our results successfully repositioned MBZ for chemoresistant HB and strongly support the use of MBZ in the next clinical trial.

ZUSAMMENFASSUNG

Das Hepatoblastom ist eine seltene Erkrankung bei Kindern mit einer niedrigen Inzidenzrate und zieht selten Aufmerksamkeit auf sich, die gegen eine konventionelle Chemotherapie resistent sind, steht die Entwicklung neuer Medikamente unmittelbar bevor. Der Zweck unseres Projekts ist es, neue, erschwingliche, wirksame und sichere Behandlungen für das Hepatoblastom zu finden.
Durch das Medikamentenvorhersage-Werkzeug CMap haben wir ein von der FDA zugelassenes Medikament, MBZ, gefunden, das von der WHO als antiparasitäres Medikament empfohlen wird.
Wir haben den Mechanismus von MBZ auf zellulärer Ebene, die Genexpression und die Proteinexpressionsebene weiter untersucht und ihn auch mit Cisplatin kombiniert, um den Behandlungsstandard zu vergleichen. Wir fanden, dass MBZ die kurz- und langfristig Zellproliferation hemmt, synergistisch in Kombination mit Cisplatin ist, die Sphärenbildung beeinträchtigt, einen G2/M-Arrest induziert, die Spindelbildung stört, Apoptose induziert, DNA-Replikations-assoziierte Gene herunterreguliert, und das Wachstum von patientennahen Sphäroid- und Xenograftmodellen reduziert. Unsere Ergebnisse zeigen eine Neupositionierung von MBZ zur Behandlung chemoresistenter HB an und unterstützen nachdrücklich die Verwendung von MBZ in der nächsten klinischen Studie.

Acknowledgment

After this thesis, my sincere thanks are due to all the members of my team who have been part of my work in our laboratory. I would like to thank Prof. Dr. Dietrich von Schweinitz and Prof. Dr. Oliver Muensterer for

the opportunity to work in the pediatric surgery department at Dr. von Hauner Children's Hospital for my dissertation.

Meticulous, gentle, and knowledgeable are not enough to describe the image of Prof. Dr. Roland Kappler in my mind, and the impact he has had on me has been tremendous. When I first entered the research field, I had no idea what to expect, but thanks to his meticulous teaching and selfless help, I was able to get started. From choosing a topic to designing an experiment to writing an article, Prof. Dr. Roland Kappler taught me the basics of scientific research with great patience and dedication.

Under the guidance of Prof. Dr. Roland Kappler, I have gradually built up my scientific system and scientific thinking. In addition, I also benefited a lot in my study and working habits, from the initial inattentiveness and carelessness to the concentration and meticulousness, and Prof. Dr. Roland Kappler gave me strict requirements at times and gentle encouragement at others. I have changed a lot during my MD life. All of what I learned from Prof. Dr. Roland Kappler will be my lifelong wealth, and the scientific spirit of Prof. Dr. Roland Kappler will guide me forward.

Special thanks to the postdoctoral fellow, Dr. Salih Demir, for his scientific research guidance. He has rich scientific research knowledge and is willing to help others. He is a role model for me on the road to scientific research. I want to thank the other members of the laboratory, Alina Hotes, Tanja Schmid, Andrei Rotari, and Negin Razizadeh for their technical and spiritual support over the years. Their friendliness and enthusiasm have given me a lot of motivation. Thanks to Yanxin Fan, Xiaohua Yang, and, Xuanwen Bao for their help during the critical period of the experiments, and every progress has been helped and witnessed by these friends. Thanks to my landlord Mr. Christian Becker, he created a relaxed and stable life atmosphere for me and solved many worries in my german life. Thanks to my friend Daniel Lüthy for seeing, accompanying, and supporting me during the low period. Thanks to my friends Xinjie Tan and Chang Liu for their consistent company, they pulled me back from the cliff, and their independence and wisdom deeply influenced me. I feel always loved. They made me who I am today. In addition, thank you for everything Munich has given me.

Because of you, I can complete my doctoral career and continue to pursue my further dreams.

Supplementary Table S1. Top 50 up and down regulated genes according to the log2fold change

Up-regulated genes	log2FoldChange	Down-regulated genes	log2FoldChange
CYP19A1	5.63043363	CD1E	-3.9367125
USH2A	4.85783348	EIF1AY	-3.8641195
NQO1	4.80613972	DES	-3.7151243
GUCY2C	4.3953521	IDO1	-3.6330565
AFP	4.15008593	ZNF667	-3.6177731
TNNC1	3.87379441	RPS4Y1	-3.4217326
ERN2	3.71209746	AKR1C4	-3.3415704
SPINK4	3.64836888	CH25H	-3.3242788
FAM153A	3.63614024	ZFY	-3.3089145
TLX1	3.61568475	FOSB	-3.2978232
HAVCR1	3.41149025	TTTY15	-3.2049902
GABRA3	3.37258708	USP9Y	-3.2036858
CRH	3.3167057	RASGRF1	-3.1726404
PAGE4	3.3148751	TBL1Y	-3.1713994
PADI1	3.30784382	EGR3	-3.1660014
CCR6	3.28502221	NLGN4Y	-3.100698
PCSK2	3.25896155	TMSB4Y	-3.0895082
PITX1	3.24575311	SCN5A	-3.0883042
KRT85	3.24416319	UTY	-3.0822538
PRSS3	3.22296949	TNFSF11	-3.053851
TFF1	3.16208795	CD247	-3.0473912
KRT31	3.14668425	SCUBE2	-3.038634
THBS4	3.12601324	LMOD1	-3.0384097
NRG1	3.10588319	CRHBP	-3.0289641
TLX2	3.09077926	IFI44L	-3.0223923
KCNC1	3.07812982	ITK	-3.012514
TFF2	3.06366087	CD207	-2.9432497
UPK3A	3.05436573	CACNA1H	-2.9374827
HOXC5	3.02283689	HMGN5	-2.9352372
BCAS1	3.01207332	TPSG1	-2.9346716
HSPA6	3.00478828	OGDHL	-2.9236862
SLC39A4	2.90830891	BCL2L10	-2.9106338
TRPC5	2.83636729	GYS2	-2.8985212
ATP6V0A4	2.8021352	NR4A3	-2.8943542

BCL2L14	2.74264905	KCNA5	-2.8934308
KCNH6	2.67999119	OLFM1	-2.8749286
SLC6A4	2.66097016	SELE	-2.8592456
CYP7A1	2.65697777	IRF4	-2.856546
SLC6A7	2.65696159	SOCS3	-2.8415934
CNR1	2.64790226	ZBP1	-2.8320924
KCNK10	2.64013078	CYP2B6	-2.8213806
ORC6	2.62256774	RTP4	-2.812677
CPLX2	2.59264479	IL2RB	-2.8091527
NAALADL1	2.56689668	IL18RAP	-2.8024675
SCARA3	2.56629808	TTTY14	-2.7966587
SOAT2	2.54805046	PYHIN1	-2.7926434
BMP7	2.53974902	ACTN2	-2.7918962
GPX2	2.49800785	ETV7	-2.7874807
ST18	2.45640631	EGR2	-2.7834949
LEFTY1	2.44319957	PRKY	-2.7656795

References

[1] A. Darbari, K. M. Sabin, C. N. Shapiro, and K. B. Schwarz, 'Epidemiology of primary hepatic malignancies in U.S. children.', *Hepatology*, vol. 38, no. 3, pp. 560–566, Sep. 2003, doi: 10.1053/jhep.2003.50375.

[2] C. E. Herzog, R. J. Andrassy, and F. Eftekhari, 'Childhood cancers: hepatoblastoma.', *Oncologist*, vol. 5, no. 6, pp. 445–453, 2000, doi: 10.1634/theoncologist.5-6-445.

[3] V. Fiaschetti, R. Fiori, E. Gaspari, S. Crusco, and G. Simonetti, 'Mixed hepatoblastoma in a young male adult: a case report and literature review.', *Case reports in medicine*, vol. 2010. p. 919457, 2010, doi: 10.1155/2010/919457.

[4] P. Sivaprakasam, A. A. Gupta, M. L. Greenberg, M. Capra, and P. C. Nathan, 'Survival and long-term outcomes in children with hepatoblastoma treated with continuous infusion of cisplatin and doxorubicin.', *J. Pediatr. Hematol. Oncol.*, vol. 33, no. 6, pp. e226-30, Aug. 2011, doi: 10.1097/MPH.0b013e31821f0eaf.

[5] A. Fucic, V. Guszak, and A. Mantovani, 'Transplacental exposure to environmental carcinogens: Association with childhood cancer risks and the role of modulating factors.', *Reprod. Toxicol.*, vol. 72, pp. 182–190, Sep. 2017, doi: 10.1016/j.reprotox.2017.06.044.

[6] K. Paquette, H. Coltin, A. Boivin, D. Amre, A.-M. Nuyt, and T. M. Luu, 'Cancer risk in children and young adults born preterm: A systematic review and meta-analysis.', *PLoS One*, vol. 14, no. 1, p. e0210366, 2019, doi: 10.1371/journal.pone.0210366.

[7] R. MacDonell-Yilmaz, K. Anderson, B. DeNardo, P. Sprinz, and W. V Padula, 'Cost-effectiveness Analysis of Screening Extremely Low Birth Weight Children for Hepatoblastoma Using Serum Alpha-fetoprotein.', *J. Pediatr.*, vol. 225, pp. 80-89.e4, Oct. 2020, doi: 10.1016/j.jpeds.2020.05.041.

[8] S. Maniar, K. Azzi, H. Iraqi, M. El Hassan Garbi, A. Chraibi, and A. Gaouzi, 'Idiopathic corporeal hemihypertrophy associated with hemihypertrichosis.', *Ann. Endocrinol. (Paris).*, vol. 72, no. 1, pp. 48–52, Feb. 2011, doi: 10.1016/j.ando.2010.06.003.

[9] G. Morcrette *et al.*, 'APC germline hepatoblastomas demonstrate cisplatin-induced intratumor tertiary lymphoid structures.', *Oncoimmunology*, vol. 8, no. 6, p. e1583547, 2019, doi: 10.1080/2162402X.2019.1583547.

[10] E. Hiyama, 'Pediatric hepatoblastoma: diagnosis and treatment.', *Transl. Pediatr.*, vol. 3, no. 4, pp. 293–299, Oct. 2014, doi: 10.3978/j.issn.2224-4336.2014.09.01.

[11] J. J. J. Gregory and J. L. Finlay, 'Alpha-fetoprotein and beta-human chorionic gonadotropin: their clinical significance as tumour markers.', *Drugs*, vol. 57, no. 4, pp. 463–467, Apr. 1999, doi: 10.2165/00003495-199957040-00001.

[12] R. Maibach *et al.*, 'Prognostic stratification for children with hepatoblastoma: the SIOPEL experience.', *Eur. J. Cancer*, vol. 48, no. 10, pp. 1543–1549, Jul. 2012, doi: 10.1016/j.ejca.2011.12.011.

[13] R. L. Meyers *et al.*, 'Risk-stratified staging in paediatric hepatoblastoma: a unified analysis from the Children's Hepatic tumors International Collaboration.', *Lancet. Oncol.*, vol. 18, no. 1, pp. 122–131, Jan. 2017, doi: 10.1016/S1470-2045(16)30598-8.

[14] D. F. Calvisi and A. Solinas, 'Hepatoblastoma: current knowledge and promises from preclinical studies.', *Transl. Gastroenterol. Hepatol.*, vol. 5, p. 42, 2020, doi: 10.21037/tgh.2019.12.03.

[15] S. Cairo *et al.*, 'A combined clinical and biological risk classification improves prediction of outcome in hepatoblastoma patients.', *Eur. J. Cancer*, vol. 141, pp. 30–39, Dec. 2020, doi: 10.1016/j.ejca.2020.09.026.

[16] A. Fonseca *et al.*, 'Extreme hepatic resections for the treatment of advanced hepatoblastoma: Are planned close margins an acceptable approach?', *Pediatr. Blood Cancer*, vol. 65, no. 2, Feb. 2018, doi: 10.1002/pbc.26820.

[17] B. J. Sunil, R. Palaniappan, B. Venkitaraman, and R. Ranganathan, 'Surgical Resection for Hepatoblastoma-Updated Survival Outcomes.', *J. Gastrointest. Cancer*, vol. 49, no. 4, pp. 493–496, Dec. 2018, doi: 10.1007/s12029-017-0005-z.

[18] D. J. Roebuck and G. Perilongo, 'Hepatoblastoma: an oncological review.', *Pediatr. Radiol.*, vol. 36, no. 3, pp. 183–186, Mar. 2006, doi: 10.1007/s00247-005-0064-3.

[19] S. Armeanu-Ebinger, A. Hoh, J. Wenz, and J. Fuchs, 'Targeting EpCAM (CD326) for immunotherapy in hepatoblastoma.', *Oncoimmunology*, vol. 2, no. 1, p. e22620, Jan. 2013, doi: 10.4161/onci.22620.

[20] P. Czauderna, D. Lopez-Terrada, E. Hiyama, B. Häberle, M. H. Malogolowkin, and R. L. Meyers, 'Hepatoblastoma state of the art: pathology, genetics, risk stratification, and chemotherapy.', *Curr. Opin. Pediatr.*, vol. 26, no. 1, pp. 19–28, Feb. 2014, doi: 10.1097/MOP.0000000000000046.

[21] E. C. Douglass, M. Reynolds, M. Finegold, A. B. Cantor, and A. Glicksman, 'Cisplatin, vincristine, and fluorouracil therapy for hepatoblastoma: a Pediatric Oncology Group study.', *J. Clin. Oncol. Off. J. Am. Soc. Clin. Oncol.*, vol. 11, no. 1, pp. 96–99, Jan. 1993, doi: 10.1200/JCO.1993.11.1.96.

[22] G. Perilongo *et al.*, 'Cisplatin versus cisplatin plus doxorubicin for standard-risk hepatoblastoma.', *N. Engl. J. Med.*, vol. 361, no. 17, pp. 1662–1670, Oct. 2009, doi: 10.1056/NEJMoa0810613.

[23] A. Makimoto, J. Fang, and H. Maeda, 'Development of a Selective Tumor-Targeted Drug Delivery System: Hydroxypropyl-Acrylamide Polymer-Conjugated Pirarubicin (P-THP) for Pediatric Solid Tumors.', *Cancers (Basel).*, vol. 13, no. 15, Jul. 2021, doi: 10.3390/cancers13153698.

[24] G. Nagae *et al.*, 'Genetic and epigenetic basis of hepatoblastoma diversity.', *Nat. Commun.*, vol. 12, no. 1, p. 5423, Sep. 2021, doi: 10.1038/s41467-021-25430-9.

[25] M. Eichenmüller *et al.*, 'The genomic landscape of hepatoblastoma and their progenies with HCC-like features.', *J. Hepatol.*, vol. 61, no. 6, pp. 1312–1320, Dec. 2014, doi: 10.1016/j.jhep.2014.08.009.

[26] Q. Wu, J. Ma, J. Wei, W. Meng, Y. Wang, and M. Shi, 'lncRNA SNHG11 Promotes Gastric Cancer Progression by Activating the Wnt/β-Catenin Pathway and Oncogenic Autophagy.', *Mol. Ther.*, vol. 29, no. 3, pp. 1258–1278, Mar. 2021, doi: 10.1016/j.ymthe.2020.10.011.

[27] J. Liu *et al.*, 'Wnt/β-catenin signalling: function, biological mechanisms, and therapeutic opportunities.', *Signal Transduct. Target. Ther.*, vol. 7, no. 1, p. 3, Jan. 2022, doi: 10.1038/s41392-021-00762-6.

[28] S. P. Monga, 'β-Catenin Signaling and Roles in Liver Homeostasis, Injury, and Tumorigenesis.', *Gastroenterology*, vol. 148, no. 7, pp. 1294–1310, Jun. 2015, doi: 10.1053/j.gastro.2015.02.056.

[29] P. Galiatsatos and W. D. Foulkes, 'Familial adenomatous polyposis.', *Am. J. Gastroenterol.*, vol. 101, no. 2, pp. 385–398, Feb. 2006, doi: 10.1111/j.1572-0241.2006.00375.x.

[30] K. Taniguchi *et al.*, 'Mutational spectrum of beta-catenin, AXIN1, and AXIN2 in hepatocellular carcinomas and hepatoblastomas.', *Oncogene*, vol. 21, no. 31, pp. 4863–4871, Jul. 2002, doi: 10.1038/sj.onc.1205591.

[31] J. Carrillo-Reixach *et al.*, 'Epigenetic footprint enables molecular risk stratification of hepatoblastoma with clinical implications.', *J. Hepatol.*, vol. 73, no. 2, pp. 328–341, Aug. 2020, doi: 10.1016/j.jhep.2020.03.025.

[32] S. Pushpakom *et al.*, 'Drug repurposing: progress, challenges and recommendations.', *Nat. Rev. Drug Discov.*, vol. 18, no. 1, pp. 41–58, Jan. 2019, doi: 10.1038/nrd.2018.168.

[33] J. Lamb *et al.*, 'The Connectivity Map: using gene-expression signatures to connect small molecules, genes, and disease.', *Science*, vol. 313, no. 5795, pp. 1929–1935, Sep. 2006, doi: 10.1126/science.1132939.

[34] J. Lamb, 'The Connectivity Map: a new tool for biomedical research.', *Nature reviews. Cancer*, vol. 7, no. 1. England, pp. 54–60, Jan. 2007, doi: 10.1038/nrc2044.

[35] X. A. Qu and D. K. Rajpal, 'Applications of Connectivity Map in drug discovery and development.', *Drug Discov. Today*, vol. 17, no. 23–24, pp. 1289–1298, Dec. 2012, doi: 10.1016/j.drudis.2012.07.017.

[36] A. Beck *et al.*, 'Connectivity map identifies HDAC inhibition as a treatment option of high-risk hepatoblastoma.', *Cancer Biol. Ther.*, vol. 17, no. 11, pp. 1168–1176, Nov. 2016, doi: 10.1080/15384047.2016.1235664.

[37] T. Pietsch, C. Fonatsch, S. Albrecht, H. Maschek, H. K. Wolf, and D. von Schweinitz, 'Characterization of the continuous cell line HepT1 derived from a human hepatoblastoma.', *Lab. Invest.*, vol. 74, no. 4, pp. 809–818, Apr. 1996.

[38] A. Ianevski, A. K. Giri, and T. Aittokallio, 'SynergyFinder 2.0: visual analytics of multi-drug combination synergies.', *Nucleic Acids Res.*, vol. 48, no. W1, pp. W488–W493, Jul. 2020, doi: 10.1093/nar/gkaa216.

[39] S. X. Ge, D. Jung, and R. Yao, 'ShinyGO: a graphical gene-set enrichment tool for animals and plants.', *Bioinformatics*, vol. 36, no. 8, pp. 2628–2629, Apr. 2020, doi: 10.1093/bioinformatics/btz931.

[40] D. Szklarczyk *et al.*, ‘The STRING database in 2021: customizable protein-protein networks, and functional characterization of user-uploaded gene/measurement sets.’, *Nucleic Acids Res.*, vol. 49, no. D1, pp. D605–D612, Jan. 2021, doi: 10.1093/nar/gkaa1074.

[41] W. Chen, C. Wong, E. Vosburgh, A. J. Levine, D. J. Foran, and E. Y. Xu, ‘High-throughput image analysis of tumor spheroids: a user-friendly software application to measure the size of spheroids automatically and accurately.’, *J. Vis. Exp.*, no. 89, Jul. 2014, doi: 10.3791/51639.

[42] D. Nicolle *et al.*, ‘Patient-derived mouse xenografts from pediatric liver cancer predict tumor recurrence and advise clinical management.’, *Hepatology*, vol. 64, no. 4, pp. 1121–1135, Oct. 2016, doi: 10.1002/hep.28621.

[43] B. Häberle, R. Maxwell, D. von Schweinitz, and I. Schmid, ‘High Dose Chemotherapy with Autologous Stem Cell Transplantation in Hepatoblastoma does not Improve Outcome. Results of the GPOH Study HB99.’, *Klin. Padiatr.*, vol. 231, no. 6, pp. 283–290, Nov. 2019, doi: 10.1055/a-1014-3250.

[44] F. Wagner *et al.*, ‘Rapamycin blocks hepatoblastoma growth in vitro and in vivo implicating new treatment options in high-risk patients.’, *Eur. J. Cancer*, vol. 48, no. 15, pp. 2442–2450, Oct. 2012, doi: 10.1016/j.ejca.2011.12.032.

[45] W. Hartmann *et al.*, ‘Activation of phosphatidylinositol-3’-kinase/AKT signaling is essential in hepatoblastoma survival.’, *Clin. cancer Res. an Off. J. Am. Assoc. Cancer Res.*, vol. 15, no. 14, pp. 4538–4545, Jul. 2009, doi: 10.1158/1078-0432.CCR-08-2878.

[46] L.-W. Ren *et al.*, ‘Benzimidazoles induce concurrent apoptosis and pyroptosis of human glioblastoma cells via arresting cell cycle.’, *Acta Pharmacol. Sin.*, vol. 43, no. 1, pp. 194–208, Jan. 2022, doi: 10.1038/s41401-021-00752-y.

[47] Q. Li *et al.*, ‘Targeting the Unwindosome by Mebendazole Is a Vulnerability of Chemoresistant Hepatoblastoma.’, *Cancers (Basel).*, vol. 14, no. 17, Aug. 2022, doi: 10.3390/cancers14174196.

[48] F. Mollinedo and C. Gajate, ‘Microtubules, microtubule-interfering agents and apoptosis.’, *Apoptosis*, vol. 8, no. 5, pp. 413–450, Oct. 2003, doi: 10.1023/a:1025513106330.

[49] J. Yue and J. M. López, ‘Understanding MAPK Signaling Pathways in Apoptosis.’, *Int. J. Mol. Sci.*, vol. 21, no. 7, Mar. 2020, doi: 10.3390/ijms21072346.

[50] H. M. Katzenstein *et al.*, ‘Minimal adjuvant chemotherapy for children with hepatoblastoma resected at diagnosis (AHEP0731): a Children’s Oncology Group, multicentre, phase 3 trial.’, *Lancet. Oncol.*, vol. 20, no. 5, pp. 719–727, May 2019, doi: 10.1016/S1470-2045(18)30895-7.

[51] J. Feng *et al.*, ‘Assessment of Survival of Pediatric Patients With Hepatoblastoma Who Received Chemotherapy Following Liver Transplant or Liver Resection.’, *JAMA Netw. open*, vol. 2, no. 10, p. e1912676, Oct. 2019, doi: 10.1001/jamanetworkopen.2019.12676.

[52] T. A. Pham, A. M. Gallo, W. Concepcion, C. O. Esquivel, and C. A. Bonham, ‘Effect of Liver Transplant on Long-term Disease-Free Survival in Children With Hepatoblastoma and Hepatocellular Cancer.’, *JAMA Surg.*, vol. 150, no. 12, pp. 1150–1158, Dec. 2015, doi: 10.1001/jamasurg.2015.1847.

[53] A. Montresor, S. Awasthi, and D. W. T. Crompton, ‘Use of benzimidazoles in children younger than 24 months for the treatment of soil-transmitted helminthiasis.’, *Acta Trop.*, vol. 86, no. 2–3, pp. 223–232, May 2003, doi: 10.1016/s0001-706x(03)00042-1.

[54] Y. Kahan, E. Lugassy-Akian, A. Ovadia, I. Dalal, E. Somekh, and D. Tasher, ‘Safety and Tolerability of Mebendazole in Infants Under 1 Year of Age.’, *J. Pediatric Infect. Dis. Soc.*, Sep. 2021, doi: 10.1093/jpids/piab077.

[55] S. K. Hegazy, G. A. El-Azab, F. Zakaria, M. F. Mostafa, and R. A. El-Ghoneimy, ‘Mebendazole; from an anti-parasitic drug to a promising candidate for drug repurposing in colorectal cancer.’, *Life Sci.*, vol. 299, p. 120536, Jun. 2022, doi: 10.1016/j.lfs.2022.120536.

[56] S. Mansoori, M. Fryknäs, C. Alvfors, A. Loskog, R. Larsson, and P. Nygren, ‘A phase 2a clinical study on the safety and efficacy of individualized dosed mebendazole in patients with advanced gastrointestinal cancer.’, *Sci. Rep.*, vol. 11, no. 1, p. 8981, Apr. 2021, doi: 10.1038/s41598-021-88433-y.

[57] J. P. Laclette, G. Guerra, and C. Zetina, ‘Inhibition of tubulin polymerization by mebendazole.’, *Biochem. Biophys. Res. Commun.*, vol. 92, no. 2, pp. 417–423, Jan. 1980, doi: 10.1016/0006-291x(80)90349-6.

[58] A. Jordan, J. A. Hadfield, N. J. Lawrence, and A. T. McGown, ‘Tubulin as a target for anticancer drugs: agents which interact with the mitotic spindle.’, *Med. Res. Rev.*, vol. 18, no. 4, pp. 259–296, Jul. 1998, doi: 10.1002/(sici)1098-1128(199807)18:4<259::aid-med3>3.0.co;2-u.

[59] A. L. Risinger and S. L. Mooberry, ‘Taccalonolides: Novel microtubule stabilizers with clinical potential.’, *Cancer Lett.*, vol. 291, no. 1, pp. 14–19, May 2010, doi: 10.1016/j.canlet.2009.09.020.

[60] P. A. Friedman and E. G. Platzer, ‘Interaction of anthelmintic benzimidazoles with Ascaris suum embryonic tubulin.’, *Biochim. Biophys. Acta*, vol. 630, no. 2, pp. 271–278, Jun. 1980, doi: 10.1016/0304-4165(80)90431-6.

[61] R.-Y. Bai, V. Staedtke, C. M. Aprhys, G. L. Gallia, and G. J. Riggins, ‘Antiparasitic mebendazole shows survival benefit in 2 preclinical models of glioblastoma multiforme.’, *Neuro. Oncol.*, vol. 13, no. 9, pp. 974–982, Sep. 2011, doi: 10.1093/neuonc/nor077.

[62] N. Doudican, A. Rodriguez, I. Osman, and S. J. Orlow, ‘Mebendazole induces apoptosis via Bcl-2 inactivation in chemoresistant melanoma cells.’, *Mol. Cancer Res.*, vol. 6, no. 8, pp. 1308–1315, Aug. 2008, doi: 10.1158/1541-7786.MCR-07-2159.

[63] V. Sudakin and T. J. Yen, ‘Targeting mitosis for anti-cancer therapy.’, *BioDrugs*, vol. 21, no. 4, pp. 225–233, 2007, doi: 10.2165/00063030-200721040-00003.

[64] K. J. Mickolajczyk, E. A. Geyer, T. Kim, L. M. Rice, and W. O. Hancock, ‘Direct observation of individual tubulin dimers binding to growing microtubules.’, *Proc. Natl. Acad. Sci. U. S. A.*, vol. 116, no. 15, pp. 7314–7322, Apr. 2019, doi: 10.1073/pnas.1815823116.

[65] A. S. Tsao and V. Papadimitrakopoulou, ‘Mitotic inhibitors.’, *J. Thorac. Oncol. Off. Publ. Int. Assoc. Study Lung Cancer*, vol. 6, no. 11 Suppl 4, pp. S1789-90, Nov. 2011, doi: 10.1097/01.JTO.0000407559.84157.c6.

[66] Q. Zang, L. Zhang, N. Gao, and C. Huang, ‘Ophiopogonin D inhibits cell proliferation, causes cell cycle arrest at G2/M, and induces apoptosis in human breast carcinoma MCF-7 cells.’, *J. Integr. Med.*, vol. 14, no. 1, pp. 51–59, Jan. 2016, doi: 10.1016/S2095-4964(16)60238-8.

[67] M. Barisic and H. Maiato, ‘The Tubulin Code: A Navigation System for Chromosomes during Mitosis.’, *Trends Cell Biol.*, vol. 26, no. 10, pp. 766–775, Oct. 2016, doi: 10.1016/j.tcb.2016.06.001.

[68] N. Pavin and I. M. Tolić, ‘Mechanobiology of the Mitotic Spindle.’, *Dev. Cell*, vol. 56, no. 2, pp. 192–201, Jan. 2021, doi: 10.1016/j.devcel.2020.11.003.

[69] X. Shu, W. Wu, R. D. Mosteller, and D. Broek, ‘Sphingosine kinase mediates vascular endothelial growth factor-induced activation of ras and mitogen-activated protein kinases.’, *Mol. Cell. Biol.*, vol. 22, no. 22, pp. 7758–7768, Nov. 2002, doi: 10.1128/MCB.22.22.7758-7768.2002.

[70] S.-H. Yang *et al.*, ‘Andrographolide induces apoptosis of C6 glioma cells via the ERK-p53-caspase 7-PARP pathway.’, *Biomed Res. Int.*, vol. 2014, p. 312847, 2014, doi: 10.1155/2014/312847.

[71] T. T. T. Nguyen, E. Tran, T. H. Nguyen, P. T. Do, T. H. Huynh, and H. Huynh, ‘The role of activated MEK-ERK pathway in quercetin-induced growth inhibition and apoptosis in A549 lung cancer cells.’, *Carcinogenesis*, vol. 25, no. 5, pp. 647–659, May 2004, doi: 10.1093/carcin/bgh052.

[72] S. Guise, D. Braguer, G. Carles, A. Delacourte, and C. Briand, ‘Hyperphosphorylation of tau is mediated by ERK activation during anticancer drug-induced apoptosis in neuroblastoma cells.’, *J. Neurosci. Res.*, vol. 63, no. 3, pp. 257–267, Feb. 2001, doi: 10.1002/1097-4547(20010201)63:3<257::AID-JNR1019>3.0.CO;2-T.

[73] L. Zhang *et al.*, ‘Identification of a panel of mitotic spindle-related genes as a signature predicting survival in lung adenocarcinoma.’, *J. Cell. Physiol.*, vol. 235, no. 5, pp. 4361–4375, May 2020, doi: 10.1002/jcp.29312.

[74] C. Janke and M. M. Magiera, ‘The tubulin code and its role in controlling microtubule properties and functions.’, *Nat. Rev. Mol. Cell Biol.*, vol. 21, no. 6, pp. 307–326, Jun. 2020, doi: 10.1038/s41580-020-0214-3.

[75] R. D’Ari, ‘Cycle-regulated genes and cell cycle regulation.’, *Bioessays*, vol. 23, no. 7, pp. 563–565, Jul. 2001, doi: 10.1002/bies.1081.

LMU LUDWIG-MAXIMILIANS-UNIVERSITÄT MÜNCHEN

Promotionsbüro
Medizinische Fakultät

MMRS

Affidavit

Li Qian

_____

Surname, first name

_____

Street

_____

Zip code, town, country

I hereby declare that the submitted thesis entitled:

In silico drug repurposing identifies mebendazole as a treatment option for chemoresistant hepatoblastoma

……

is my own work. I have only used the sources indicated and have not made unauthorised use of services of a third party. Where the work of others has been quoted or reproduced, the source is always given.
I further declare that the submitted thesis or parts thereof have not been presented as part of an examination degree to any other university.

Munich 20.01.2023

_____

place, date

Qian Li

_____

Signature doctoral candidate